THE ROLE OF SURFACE-WAVE BREAKING IN AIR-SEA INTERACTION

W. K. Melville

Scripps Institution of Oceanography, University of California, San Diego, La Jolla, California 92093-0213

ABSTRACT

Breaking serves to limit the height of surface waves, mix the surface waters, generate ocean currents, and enhance air-sea fluxes of heat, mass, and momentum through the generation of turbulence and the entrainment of air. Breaking may result from intrinsic instabilities of deep-water waves or through wave-wave, wave-current, and wind-wave interactions. Observations in the field are made difficult by the fact that breaking is a strongly nonlinear intermittent process occurring over a wide range of scales. Controlled laboratory studies of breaking have proven useful in measuring the scaling relationships between the surface wave field and the kinematics and dynamics of breaking. Our inability to predict the occurrence and dynamics of breaking is a major impediment to the development of better wind-wave and mixed-layer models. Modern acoustic and electromagnetic oceanographic instrumentation should lead to significantly improved measurements of breaking in the near future.

1. INTRODUCTION

The study of surface waves has a long tradition in theoretical and applied mechanics. Even before the formal investigation of the subject it must have been of interest for as long as man has been involved in fishing, maritime exploration, and trade. The dangers presented to early explorers by wind and

279

waves are readily apparent when it is observed that many were putting to sea
in ships barely longer than most contemporary cruising yachts. Even today,
fishing vessels capsize and are lost in steep and breaking seas. Although steep
and breaking seas provide the extreme environments that are encountered, it is
still the case that most descriptions of the ocean surface, whether for engineering
or oceanographic purposes, are based on linear theory. The foundations of linear
wave theory were laid by many of the founders of theoretical hydrodynamics
in the nineteenth century. In 1847 Stokes published his investigation of weak
nonlinear effects on surface waves, but it took a century for the subject to extend
to an investigation of nonlinear interactions between surface waves (Miche
1944, Longuet-Higgins & Ursell 1948, Phillips 1960, Hasselmann 1962) and
subsequently the stability of weakly nonlinear deep-water waves (Lighthill
1965, Benjamin & Feir 1967).

Convenient measures of the nonlinearity are the wave steepness ak, where a is
the wave amplitude (half the trough-to-crest distance) and k is the wavenumber,
or equivalently, u/c, where u is a measure of the horizontal fluid velocity at
the surface and c is the phase speed. In breaking waves u/c may exceed unity
while ak is of $O(1)$, and so breaking is a strongly nonlinear process. Rigorous
theoretical investigations of breaking have been confined to describing local
features of the flow (for a review see Longuet-Higgins 1988). Numerical codes
are available to describe the evolution of two-dimensional surface waves up
to breaking, but they are unable to continue beyond the point at which the
surface impacts on itself (Dommermuth et al 1987). Thus the study of wave
breaking is based in large part on experiments in both the laboratory and the
field, supplemented by process-oriented models.

The most obvious expression of breaking at the sea surface is a whitecap
caused by entrained air. (See Monahan & McNiocaill 1986.) Whitecaps be-
come evident at scales of $O(1\text{ m})$ extending up to $O(100\text{ m})$, but breaking may
occur without significant air entrainment down to scales of centimeters. This
lack of a universal visual feature identifying breaking and the difficulty of mea-
suring variables in a two-phase, free-surface turbulent flow have made progress
difficult, especially in the field. However, attempts at confronting this difficulty
are justified by the importance of breaking for the processes occurring at the
air-sea interface. Breaking plays a number of related roles in air-sea interaction.
These include:

- limiting the height of surface waves,

- being a source of vorticity and turbulence,

- dissipating surface-wave energy, some of which is available for turbulent
  mixing,

- generating ocean currents by transferring momentum flux from the wave field,

- enhancing gas transfer via surface turbulence and bubble entrainment,

- generating sound at the ocean surface that can be used as a diagnostic tool for air-sea interaction studies (acoustical oceanography), and

- providing passive and active microwave signatures that may prove useful in remote sensing of the ocean.

It may seem surprising that a process that is intermittent in space and time, and that, at least at the larger scales, is only occurring over a small fraction of the ocean surface at any time, may be significant. We see below that the direct effects of breaking are typically felt to a depth of the order of the wave height. In relatively benign conditions this may be to depths of the order of meters, but in stormy seas this region may extend to depths of $O(10 \text{ m})$. The sensitivity of the atmosphere-ocean system to the conditions in the upper ten meters of the ocean are graphically presented by Gill (1982):

- Of the solar radiation incident on the atmosphere, 40% is absorbed in the first 10 m of the ocean; more in coastal waters.

- The first 10 m of the water column has the same weight as all the atmosphere above.

- The first 2.5 m of the water column has the same heat capacity as all the (dry) atmosphere above.

Breaking generating whitecaps is observed to begin at a wind speed of approximately 3 m s^{-1} (6 knots). Now the momentum and mechanical energy fluxes across the air-sea interface typically scale as the square and cube of the wind speed, respectively, so even relatively short periods of high winds and waves may contribute significant fractions of the total fluxes across the air-sea interface, with breaking absent only under the most benign conditions. For example, with the transport rate proportional to the cube of the wind speed, the mechanical energy transferred across the sea surface during one week of 40-knot winds is approximately equivalent to that in one year of 11-knot winds!

I review some of the recent contributions to our knowledge of breaking and its role in air-sea interaction. This is not meant to be an exhaustive review of the subject, a task that would expand well beyond the space available. However, it is hoped that the reader will achieve an appreciation for the wide range of problems that remain to be solved and the techniques that are being brought to bear.

Several reviews of wave breaking and related topics have appeared in recent years, including one on deep-water wave breaking in this series just three years ago (Banner & Peregrine 1993). Where feasible I have attempted to not unnecessarily duplicate material presented by Banner & Peregrine. Thorpe (1992, 1995) has written excellent reviews of the surface bubble layer and the dynamics of the ocean surface layer, respectively. This article is a significant revision of a recent review of the same subject by the author (Melville 1993). Because this is a very active area of research, it is unlikely that any review will remain current for more than a few years.

2. ROUTES TO BREAKING

Stokes' periodic wave of highest slope ($ak = 0.4432$) with its 120° corner flow has in the past been considered as a model of breaking. In a frame of reference traveling at the phase speed the fluid at the crest is at rest, and so in the laboratory frame it is moving at the phase speed of the wave. This then satisfies the kinematic breaking criterion that the fluid velocity matches or exceeds the phase velocity. However, it is most unlikely that such a flow can ever be realized, since uniform wave fields of much smaller slope are subject to intrinsic instabilities, which may lead to breaking. Melville (1982) has shown experimentally that for wave slopes below approximately 0.3, two-dimensional uniform wave trains are unstable to two-dimensional Benjamin-Feir instabilities, which ultimately lead to breaking, while at larger slopes rapid three-dimensional instabilities dominate (see also Yuen & Lake 1980, Su et al 1982, McLean et al 1981). [The graphic photograph of three-dimensional instabilities by Su et al (1982) has done much to draw attention to the subject.] Numerical solutions have shown that uniform wave trains with slopes as small as 0.1 may evolve to breaking following Benjamin-Feir instability (Dold & Peregrine 1986; see also Longuet-Higgins & Cokelet 1978). Stability analyses of uniform wavetrains have demonstrated the possibility of various instability mechanisms for wave slopes less than 0.4432, some of which may lead to breaking (Longuet-Higgins & Cleaver 1994, Longuet-Higgins et al 1994).

Laboratory experiments by a number of authors (see Bonmarin 1989) have shown that breaking may occur for values of the wave height H and period T having a dimensionless wave-height parameter H/gT^2 as small as 0.01,[1] which is to be compared with a value of 0.027 for Stokes' limiting wave. However, there is much scatter in the data. Although global measures of the slope at breaking (ak, H/gT^2) may be quite modest, the local slope may become infinite, especially in overturning surfaces that entrain air. Thus, criteria for

---

[1]Note that $H/gT^2 = ak/(2\pi^2)$ for $ak \ll 1$.

breaking based on slope, if valid at all, are clearly scale dependent. This presents great experimental difficulties since there are no methods available for measuring the evolution of the spatial structure of water surfaces over a wide range of scales and slopes.

Waves may break as a result of constructive interference, wave-wave, wave-current, and perhaps wind-wave interactions (Figure 1). The dispersive properties of surface waves and their directional distribution on the ocean surface leads to modulation of the wave envelope. In the simplest case of linear wave propagation in one direction the envelope and wave energy travels at the group speed $c_g = \sigma/2k$, which is half the linear phase speed, so that wave crests enter the rear of the group and exit at the front. Donelan et al (1972) observed the consequences of this process with waves periodically breaking as they passed through the group. Dispersion can lead to focusing of wave energy in a relatively small region, with the result that waves break in an unsteady manner. This can be produced in the laboratory by first generating high-frequency waves followed by lower-frequency waves and then adjusting the rate of change of frequency according to the linear group velocity to give focusing at a point down the channel (Longuet-Higgins 1974). This process has proved useful to generate whitecaps (Melville & Rapp 1985) in which the wave crest propagates forward and impacts on the surface below, entraining a volume of air that then breaks up into a cloud of bubbles (Figure 2; Lamarre 1993). Most recently, the constructive interference technique has been used to carefully investigate the threshold of breaking (Duncan et al 1994a,b). Flow visualization shows that at large crest curvatures a toe is formed on the forward face of the wave. The even higher curvature at the toe of the disturbance rapidly leads to the generation of parasitic capillaries, which grow and evolve into a turbulent spilling region on the forward face of the wave (Figure 3). Longuet-Higgins & Cleaver (1994) have found that the formation of the initial toe is similar to an inviscid irrotational instability of the "almost highest" wave (see also Longuet-Higgins et al 1994). The large curvature at the tip of the toe along with the free-surface boundary conditions lead to the generation of vorticity associated with the capillary waves. This vorticity is then transported into the surface layers and, with the image vorticity in the surface, may resonate with free-surface modes (Longuet-Higgins 1994). This model, while plausible, remains to be tested more rigorously against the empirical data. Laboratory measurements also suggest that the Benjamin-Feir instability generates dispersive sideband components that may lead to gentle breaking through constructive interference or focusing (Melville 1982, 1983).

Modeling and measurements presented below suggest that much of the breaking in the wind-generated wave field is at frequencies greater than the peak of the
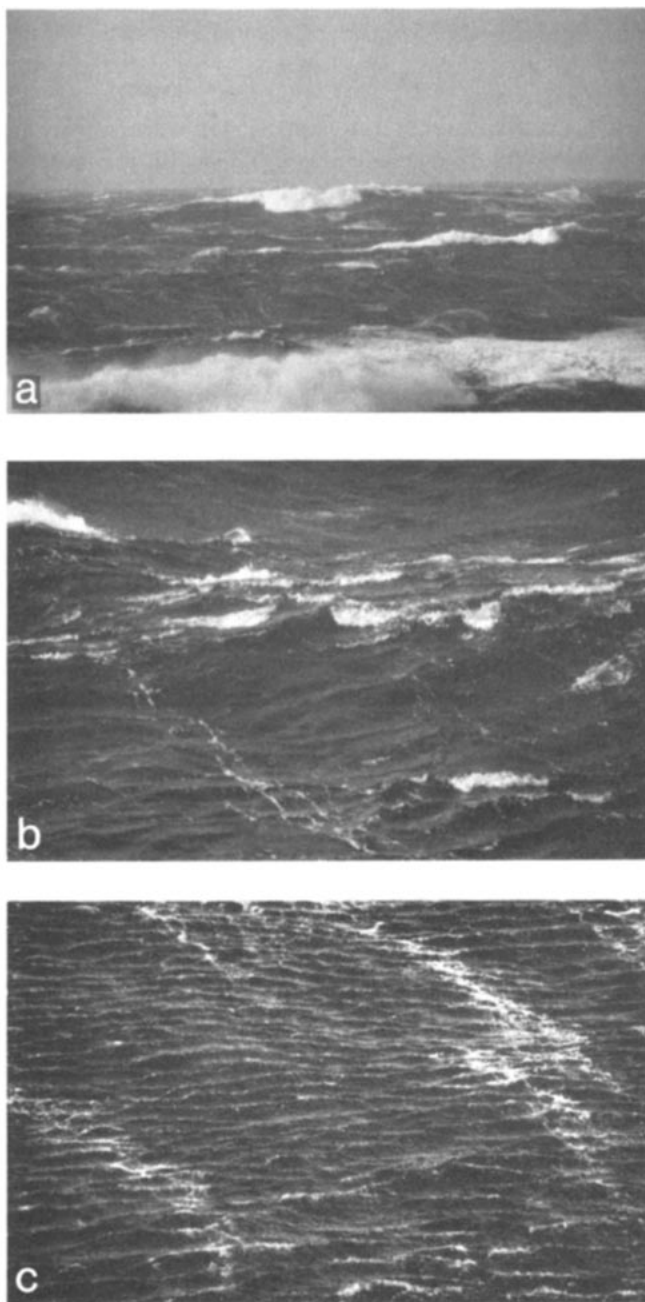
Figure 1   Examples of wave breaking from a storm in the North Atlantic in December 1993 in which the winds were gusting up to approximately 50–60 knots and wave heights of up to 12–15 m were reported. (*a*) Large-scale breaking waves. (*b*) Smaller-scale waves breaking on longer waves. (*c*) Short, strongly wind-forced breaking waves. (Photographs by E Terrill & WK Melville.)
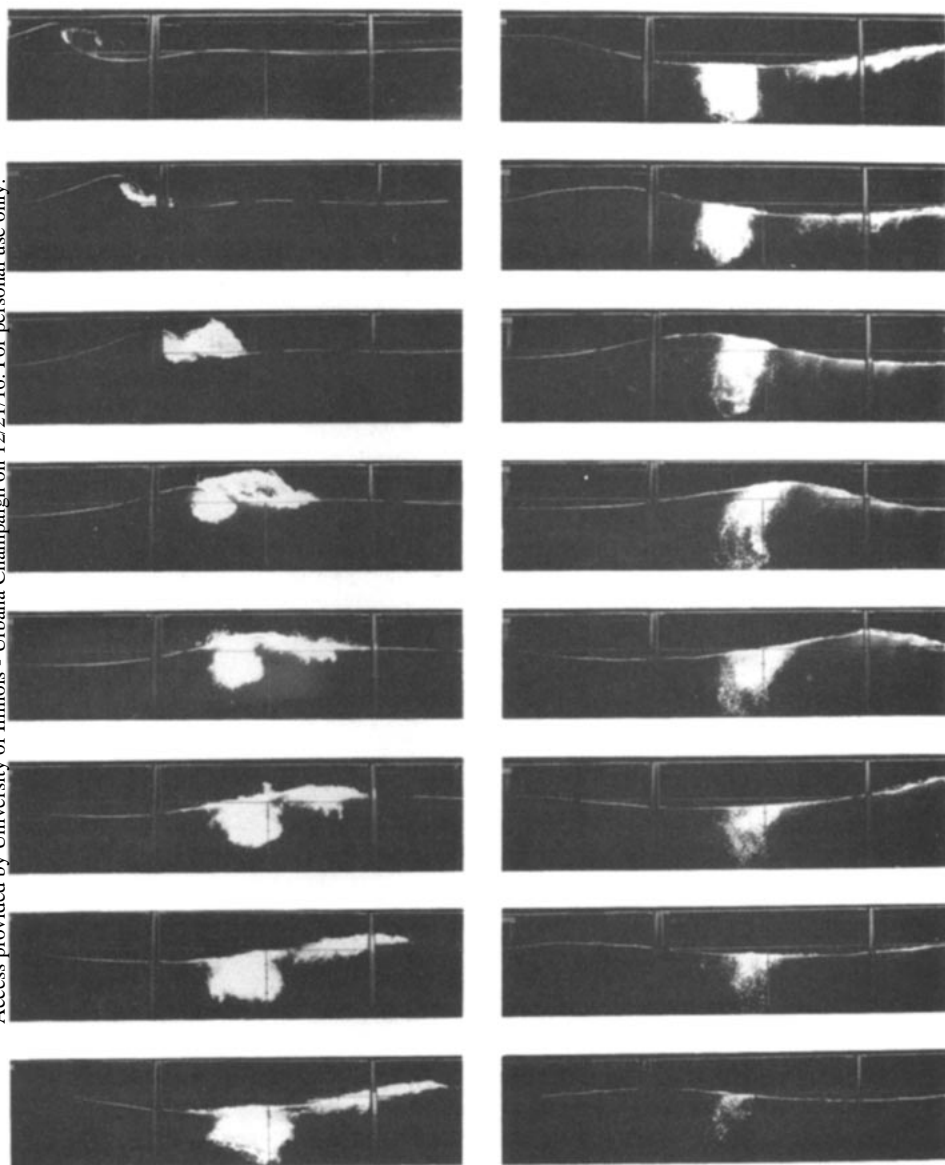
Figure 2   Generation of a plunging breaking wave in the laboratory showing significant air entrainment and degassing as the larger bubbles rise back to the surface. (From Lamarre 1993.)
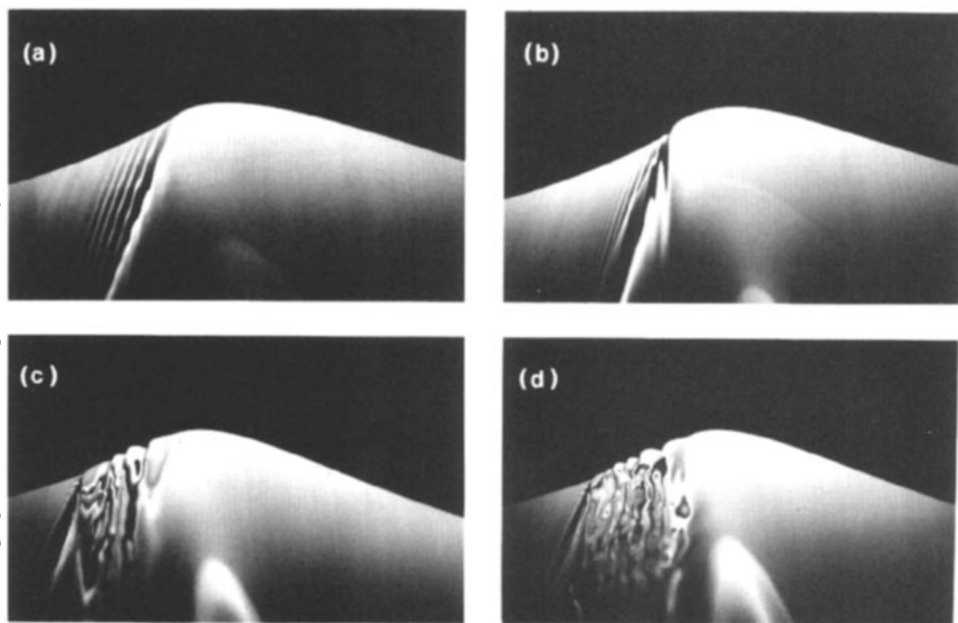
Figure 3   Generation of a gently breaking wave in the laboratory. Note the generation of the toe in (*a*) forward of the crest followed by the growth of parasitic capillary waves. (From Duncan et al 1994b.)

spectrum. These shorter gravity waves propagate on and are modulated by the longer gravity waves of slope AK. Extending earlier work of Longuet-Higgins & Stewart (1960, 1964) and Phillips (1981) for $AK \ll 1$, Longuet-Higgins (1987) considered linear short waves propagating on a nonlinear long wave in a frame moving at the phase speed of the longer waves. Using numerical solutions for the longer wave permitted the calculation of the effective gravity felt by the shorter waves, which along with action conservation led to predictions of the modulation of the slope ak of the shorter waves. The numerical results showed that for $AK = 0.3$, the ratio of the slope of the short waves at the crest to the slope at the trough could be as great as 4. According to these results a short-wave slope as small as 0.075 at the trough could be amplified to a slope of 0.3 at the crest. Uniform waves of this steepness are unstable to rapid three-dimensional instabilities, leading to breaking. Subsequent analytical and numerical work by Zhang & Melville (1990, 1992) showed that these steady solutions are unstable if the nonlinearity of the short waves is taken into account. Although this theoretical problem has been treated in an idealized

two-scale approach, in nature we would expect a heirarchy of multiple-scale interactions between shorter wind waves or gravity-capillary waves and longer waves or swell (cf Figure 1*b*). Laboratory experiments on long-wave/short-wave interactions leading to breaking have been reported by Longuet-Higgins (1988). (See also Miller et al 1991.)

It is well known that waves propagating against an increasing current may steepen and break (Longuet-Higgins & Stewart 1964). This may be commonly observed as wind waves propagate toward the mouth of an estuary at ebb tide or against a strong rip current near the shore. Some of the most dramatic examples of this effect are associated with surface signatures of long nonlinear internal waves in marginal seas or ocean fronts. Osborne & Burch (1980) showed sunglint photographs from the *Soyuz* spacecraft and corresponding photographs from a ship as large internal waves propagated across the Andaman Sea. The ship photographs showed clear bands of short breaking waves propagating with the internal waves. The initial stages of this wave-current interaction, which ultimately lead to a modulation to breaking of the shorter waves, can be described by wave action conservation. Recent field experiments have shown similar breaking phenomena along coastal and equatorial fronts. Indeed, we may anticipate that any oceanic or atmospheric process that leads to significant strain rates of the surface currents may also induce modulation to breaking of the surface waves.

In the examples cited above the wind has been considered not to play a dominant role—the time scale for wind-wave growth is significantly longer than that for the more rapid local breaking. However, observation of the ocean surface at higher wind speeds reveals the presence of short waves of $O(0.1-1 \text{ m})$ in length that appear to be strongly wind forced, turbulent, asymmetric (with steeper forward faces), and almost continuously breaking (cf Figure 1*c*). They have the appearance of trains of bores propagating on a turbulent surface layer and perhaps constitute the aerodynamic roughness elements for the atmospheric boundary layer above. As far as we are aware no work has been done on these very short wind-forced breaking waves, but Banner & Phillips (1974) have considered the effect of a thin laminar wind-drift layer in reducing the amplitude at which waves break.

3. OBSERVATIONS OF BREAKING WAVES

Field observations of breaking have been based on detecting large temporal gradients in the surface displacement (the "jump meter"; Longuet-Higgins & Smith 1983, Thorpe & Humphries 1980) and relating them to surface slope through the phase speed of the wave. Waves with slopes exceeding a particular threshold were considered to be breaking. In addition to other problems, this method of detection is complicated by the scale dependence mentioned
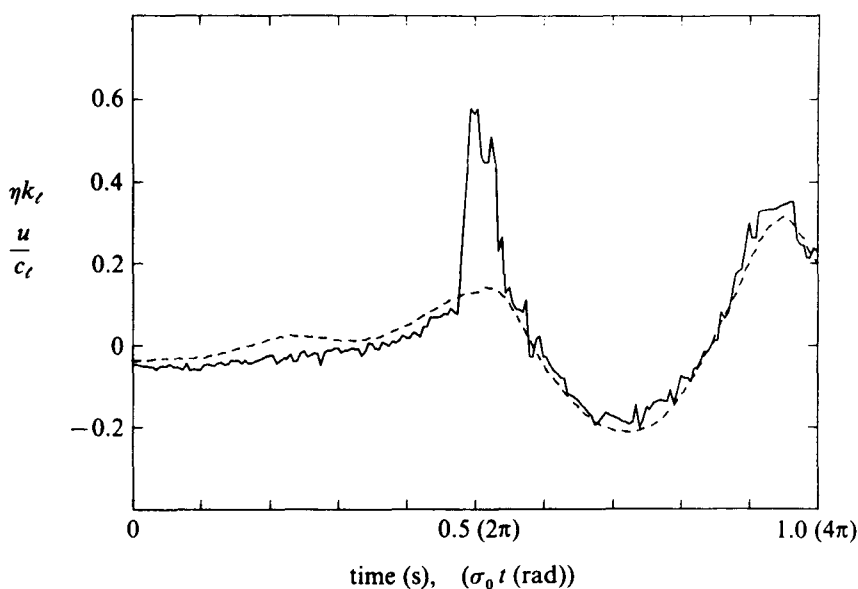
above. Weissman et al (1984) used high-passed wave-gauge time series to detect breaking in lake experiments. Because large temporal gradients are resolved by high-frequency Fourier components, the jump-meter and high-pass filter approaches are closely related. Holthuijsen & Herbers (1986) visually observed whitecaps at the location of a wave-measuring buoy and analyzed their data in terms of the joint height-period probability distributions of both the broken and unbroken waves passing the buoy. These distributions showed considerable overlap and no clear threshold for breaking based on the combined wave height and period. The difficulty with point measurements, whether in the laboratory or field, is that in a random breaking wave field they may catch the wave at any stage in the breaking process, and because the wave parameters may change during breaking they are not necessarily the same as those at the onset of breaking.

This point has been made very clear by laboratory studies. Melville & Rapp (1988) used a laser Doppler velocimeter (LDV) to measure the horizontal velocity of the fluid at the surface and to detect breaking. Figure 4 shows an example of a small section of coincident surface displacement and velocity time

Figure 4 Laboratory measurements of the normalized surface displacement (*dashed line*) and horizontal fluid velocity component (*solid line*) in breaking and unbroken waves following Benjamin-Feir instability of a uniform wave train. (From Melville & Rapp 1988.)

series. Of the two waves in the frame, the smaller less-steep wave is breaking while the larger steeper wave is not. The wave began breaking near the peak of the wave envelope but decreased in amplitude and slope as it continued to break. Bonmarin's (1989) laboratory measurements showed significant changes in the wave parameters during breaking. These examples demonstrate the danger of using observations of breaking at an undetermined stage in its evolution to infer breaking criteria. It also points to the difficulties inherent in using the surface displacement at a point or its first derivative in time as an accurate indicator of breaking.

The intermittent random occurrence of breaking in the field is clearly not well described by isolated point measurements. Breaking is better observed by measuring related variables as a function of two-dimensional position on the ocean surface as they evolve in time. Phillips (1985) proposed that the statistics of breaking be described by a distribution function $\Lambda(c)$ such that $\Lambda(c)dc$ represents the average total length of breaking fronts, per unit area of ocean surface, that have speeds in the range c to $c + dc$. The total length of breaking fronts per unit area is then

$$L = \int_0^\infty \Lambda(c)dc \tag{1}$$

and the fraction of the total surface area swept over per unit time by breaking waves is

$$R = \int_0^\infty \Lambda(c)c\,dc, \tag{2}$$

where the distribution $c\Lambda(c)dc$ gives the expected number of breaking events with velocities in the range c to $c + dc$ passing a fixed point per unit time. It is also apparent that the geometry and kinematics of the surface may not be the most appropriate measurements in all cases. In many instances the process of interest (e.g. heat transfer, gas transfer, turbulent mixing) may dictate the most appropriate diagnostic variable to use as an indicator of breaking. This sidesteps the contentious hydrodynamic issue of whether or not there is a "universal" breaking criterion. For example, if the heat transfer associated with breaking is the issue, then thermal images of the mixing of cooler (warmer) water across the warmer (cooler) surface layer may be the direct measurement of interest. Figure 5 shows an example of just such an infrared image taken by Jessup (1995). In laboratory measurements Rapp & Melville (1990) used the mixing down of a dyed surface to both detect breaking and to quantify the turbulent length and velocity scales of the mixing. Similar analyses may be used on infrared images.

In recent years other nonhydrodynamic methods of detecting breaking have been investigated and exploited. These include acoustic methods and microwave

methods. The use of active microwave methods to detect and quantify breaking has been investigated by a number of authors. Keller et al (1986) presented an illustrative summary of the use of coherent microwave systems in measuring breaking waves. They pointed out that specular, Bragg, and volume scattering may contribute to the scattered components. Banner & Fooks (1985) associated enhanced scattering by a quasi-steady spilling wave with the Bragg components in the smaller-scale waves and surface disturbances that accompany the turbulence. The author and his co-workers (Melville et al 1988; Jessup et al 1990, 1991a,b; Loewen & Melville 1991a) have attempted to quantify the scattering by breaking waves and correlate it with the dynamics of breaking. In laboratory studies we have found that the scattering correlates with the dissipation due to breaking, although the detailed reason for this result remains to be investigated. In the field we have found that the lower-order moments of the microwave Doppler spectrum taken together provide a good indicator of breaking and that the contribution of the breaking waves to the radar cross section at moderate incidence angles is significant and increases approximately as the cube of the friction velocity of the wind, consistent with modeling of Phillips (1988). Nevertheless, the fact remains that steep but unbroken waves may have similar microwave signatures to breaking waves, and resolving the differences may prove difficult, especially with small footprint scatterometers. However, recent advances have led to the use of FMCW (frequency modulated continuous wave) radars (Smith et al 1995) and phased-array radars (Frasier et al 1995) for ocean imaging. The imaging radar can give two-dimensional scatterer velocity and radar cross-section images of the ocean surface at a spatial resolution of $O(1 \text{ m})$ at $O(10 \text{ Hz})$ for areas of $O(10^4–10^5 \text{ m}^2)$. This ability to monitor the evolution of radar images and hence breaking-wave signatures in two-dimensional space and time should greatly enhance our attempts to use radars for detecting and quantifying breaking.

Acoustics is another powerful tool, and we have more to say on this subject later. The entrainment of air by breaking leads to the radiation of sound from the breaker; the injected bubble cloud also presents a strong acoustic scatterer. Thus both passive and active acoustical techniques can be used to identify and track breaking waves. Thorpe and his associates have pioneered the use of active acoustics for identifying breaking waves by deploying side-scan sonars at lake and coastal sites (Thorpe & Hall 1983). This technology has been further developed by Pinkel & Smith (1987), who added a Doppler capability and multiple beams. Scattering from the surface bubble clouds may then be used to measure the directional wave spectrum as well as identify intermittent regions of larger backscatter and Doppler shift associated with breaking-induced bubble injection events.

Crowther & Hansla (1993) have used a seven-element directional hydrophone array along with video imaging from a helicopter to acoustically identify and track breaking waves. These were clearly preliminary measurements for proof of the technique and did not have the supporting environmental measurements to permit firm conclusions to be drawn; however, they did show that breaking waves could be tracked acoustically, that the acoustic technique detected events that went undetected in video recordings of whitecaps, and that the approximate acoustic shape of the breaker could be resolved. Using a small hydrophone array suspended below a surface float, Ding & Farmer (1994a) have identified, quantified, and tracked breaking waves by measuring the sound they radiate. With a relatively small hydrophone array they were able to measure the speed and duration of the breaking events and correlate them with the other environmental measurements. The results of their measurements are discussed below.

In summary, the only reliable hydrodynamic methods for identifying breaking at all scales include measurements of both the surface geometry and the velocity field at the surface. Such methods are confined to the laboratory at present. The problem of detection and quantification of the parameters describing breaking waves remains an impediment to field studies of breaking, but significant progress has been made in recent years and much more can be expected in the very near future.

4. MOMENTUM FLUX ACROSS THE AIR-SEA INTERFACE

Even to the casual observer it is obvious that the wind generates waves and currents. What is not so obvious is the partitioning of the fluxes across the air-sea interface between waves and currents. Surface waves have an associated mean momentum flux that is proportional to the square of the wave height. If the waves were to continuously receive momentum from the wind they would continue to grow and the momentum flux they carry would continue to increase. The growth of the waves is arrested by breaking, and in breaking the wave field gives up part of its momentum flux to currents. Thus breaking is an important process in the generation of ocean currents.

The partitioning of stress in the atmospheric boundary layer between turbulent Reynolds stresses and wave-induced stresses and their dependence on sea state is an area of significant interest to wind-wave modelers and those developing parameterization schemes for coupled atmosphere-ocean models. In the context of surface-wave breaking, one of the central issues was clearly stated by Mitsuyasu (1985). The essentials may be discussed by considering a locally uniform two-dimensional wave field that has spatial gradients on a scale much

larger than the wavelength. The wave momentum flux S_{11} is given by

$$S_{11} = \frac{1}{2}E, \qquad (3)$$

where $E = \rho_w g a^2/2$ is the wave energy density and ρ_w is the density of the water. The momentum flux from the air to the water τ_0 is given by $\tau_0 = \tau_w + \tau_t$, where τ_w is the flux directly into the waves and τ_t is the remaining turbulent flux that is not coherent with the wave field. In the absence of dissipation, τ_w can be related to the gradient in the momentum flux due to wave growth,

$$\tau_w = \frac{dS_{11}}{dx} = \frac{\beta}{c}E, \qquad (4)$$

where $\beta = (c_g/E)(dE/dx)$ is the energy density growth rate and c and c_g are the phase and group velocities, respectively. From laboratory experiments in the absence of breaking, Mitsuyasu (1985) found that $\tau_w = 22(ak)^2\tau_0$, which gives significant values of $\tau_w/\tau_0 \approx 0.35$ for representative values of the wave slope $ak \approx 0.13$. This estimate of the momentum flux directly into the wave field was supported by laboratory and field measurements, giving τ_w/τ_0 in the range 0.4–0.6 (Hsu et al 1981, 1982; Snyder et al 1981). However, field measurements of the secular wave growth showed that $(dS_{11})/(dx) = 0.05\tau_0$; that is, only 5% of the momentum flux from the atmosphere is carried by waves propagating out of the generation region. This is approximately 10% of the measured momentum flux from the wind to the waves. Mitsuyasu conjectured that the remainder of τ_w is lost from the wave field by breaking in the generation region. More detailed modeling and data (Komen et al 1994) suggest that for young wind seas[2] ($c_p/u_{*a} \leq 5$), $\tau_w/\tau_0 \approx 1$. This flux ratio decreases to approximately 0.5 for $c_p/u_{*a} = 25$, but the essential result remains.

The above argument was supported by laboratory experiments on unsteady breaking by Melville & Rapp (1985). Using the dispersive properties of deep-water waves to focus a wave packet in a laboratory channel, and by measuring the wave field upstream and downstream of the break, we measured the excess momentum flux lost from the wave field. (See Figure 6a.) Using field measurements of the incidence of breaking by Thorpe & Humphries (1980), it was shown that Mitsuyasu's conjecture was supported by the combined laboratory and field data. Rapp & Melville (1990) extended the laboratory studies considerably. We can conclude from this work that although a significant fraction of the momentum flux from the atmosphere may pass through the wave field (50% or more), most of it is lost to currents by breaking in the generation region.

---

[2]The "age" of the sea is given by the ratio of the phase speed at the peak of the spectrum c_p to the friction velocity in the air u_{*a}.

5.   WIND-WAVE MODELING

5.1   *The Radiative Transfer Equation*

A rigorous theoretical foundation for prediction of wind-wave generation evolution and decay does not yet exist, but a sufficient number of the important pieces of the puzzle can be assembled to formulate the problem in terms of the radiative transfer equation (Phillips 1977, Komen et al 1994):

$$\frac{dN}{dt} = \frac{\partial N}{\partial t} + (\mathbf{c_g} + \mathbf{U}) \cdot \nabla N = -\nabla_k \cdot \mathbf{T(k)} + S_\mathrm{w} - D, \tag{5}$$

where $N(\mathbf{k}) = gF(\mathbf{k})/\sigma = (g/k)^{1/2}F(\mathbf{k})$ is the wave action spectral density; $\mathbf{T(k)}$ is the action spectral flux due to wave-wave interactions; S_w is the wind input; and D represents the dissipation, which is thought to be due primarily to breaking. $I \equiv -\nabla_k \cdot \mathbf{T(k)}$ is the "collision integral" representing the nonlinear wave-wave interactions as formulated by Hasselmann (1962).

Parameterizing S_w and D and efficiently computing I comprise the crux of the wind-wave prediction problem. This is an area of both basic and applied research, with fundamental questions obscured by the commonly accepted parameterizations that are necessary to arrive at tractable (numerical) solutions to practical problems. For an excellent up-to-date treatment the reader is referred to Komen et al (1994), who show that the subject has developed in much the same way as turbulence modeling with a combination of rigorous idealized models, physically motivated approximations and parameterizations, and empirically based "constants" being used to give closure. The cornerstones of the modeling are the rational theories of wind-wave generation and nonlinear wave-wave interactions. The wind-input term is based on Miles' theory (1957, 1993) and empirical input (Snyder et al 1981, Plant 1982), leading to an expression of the form

$$S_\mathrm{w} = m\cos^{2p}\theta\sigma(u_{*\mathrm{a}}/c)^2 N(\mathbf{k}) \tag{6}$$

(Phillips 1985), where m and p are empirical constants and $u_{*\mathrm{a}}$ is the friction velocity in the air.

The nonlinear wave-wave interaction term I is derived on the basis of a small-slope approximation for gravity waves in the energy containing part of the spectrum and is typically limited to considering quartet interactions in the neighborhood of the resonant manifolds. Closure is based on a Gaussian assumption, which leads to certain subtleties in the reversibility of the process of wave evolution and an inability to consider interactions between waves of disparate scales. This excludes the important long-wave short-wave interactions discussed above, which are important for inverting remotely sensed microwave
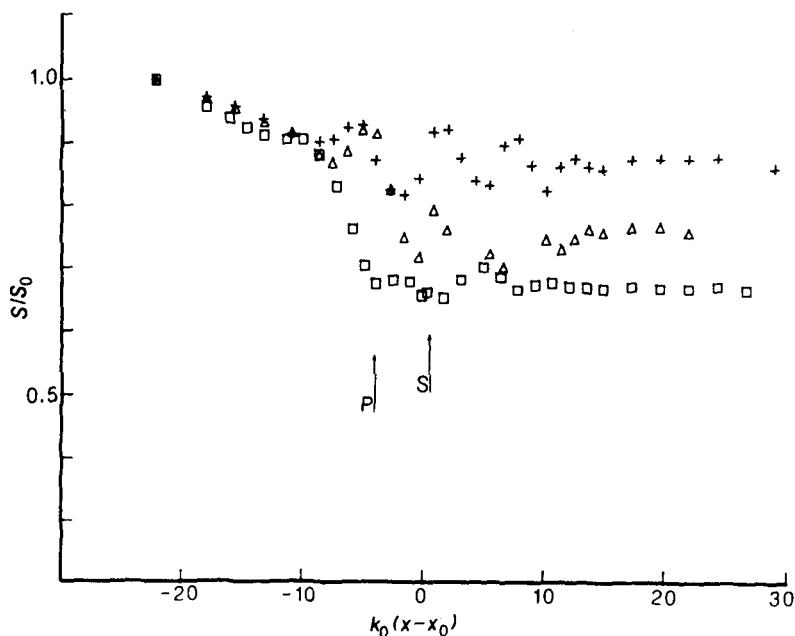
a

Figure 6   Laboratory measurements of the decrease in the normalized variance of the free-surface displacement of a wave packet due to breaking. (*a*) Normalized variance as a function of the normalized distance downstream. S and P mark the breaking positions of single spilling and plunging waves, respectively. (*b*) The normalized difference across the breaking region determined from data similar to that in (*a*). This quantity is proportional at lowest order to both the loss of excess momentum flux and energy from the wave packet. Note that a_0 and k_0 are measures of characteristic wave amplitude and wave numbers, respectively. [From Melville & Rapp 1985.] Reprinted with permission from *Nature*. Copyright (1985) Macmillan Magazines Limited.

data. Exact numerical computation of I is typically limited to research problems; operational wind-wave models normally use an approximate form of I, which, for example, may assume that the dominant interactions are between neighboring wavenumbers.

The dissipation term is the least well understood. By assuming that wave breaking is equivalent to surface pressure perturbations that are local on space and time scales small compared to the respective scales of the breaking waves, Hasselmann (1974) found that if the dissipation term was also weak in the mean, then it was proportional to the spectral energy density with a damping coefficient proportional to the square of the wave frequency. This result, subsequently
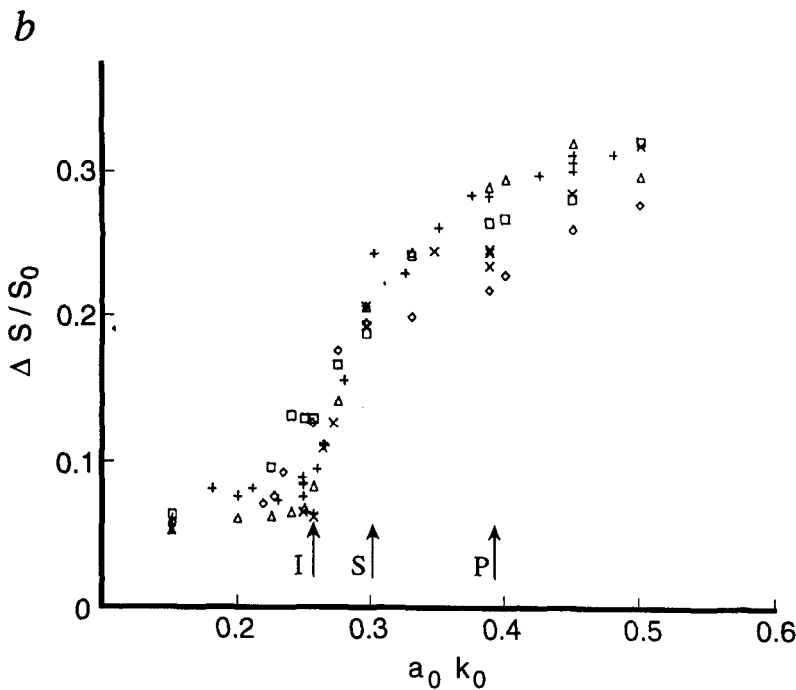
b

Figure 6 *(continued)*

modified by Komen et al (1984), leads to an expression of the form

$$D \propto \bar{\sigma}(\sigma/\bar{\sigma})^2(\hat{\alpha}/\hat{\alpha}_{PM})^2 N(\mathbf{k}), \tag{7}$$

where σ is the radian frequency, $\hat{\alpha}$ is a slope parameter, and the subscript "PM" refers to a value representative of the fully developed spectrum (Pierson & Moskowitz 1964). Overbars denote mean quantities. Figure 7 shows an example of the spectrum and the contributions from the various terms as computed by Komen et al (1984). According to this model the wind input and dissipation predominate at frequencies greater than the spectral peak, whereas the effect of the nonlinear interactions is to add energy at the lower frequencies while subtracting it from the higher frequencies. Clearly, if this class of models is representative of the physics, then the dissipation due to breaking is comparable to the wind input and must have a profound effect on the details of the spectral evolution (see Trulsen & Dysthe 1992).

A less direct influence of breaking is on the wind-input term itself. Breaking may also enhance the momentum flux from the atmosphere to the ocean

through air-flow separation that is concomitant with quasi-steady breaking and modifies the phase of the aerodynamic pressure relative to the surface wave (Banner & Melville 1976, Banner 1990a, Banner & Peregrine 1993). However, these effects require more measurements in unsteady breaking to confirm the significance of the phenomenon over a range of scales at the ocean surface.

5.2   Equilibrium Models and Spectral Slopes

Numerical solutions of the wind-wave model equations, like the results of physical experiments, need interpretation. With the example of the success of
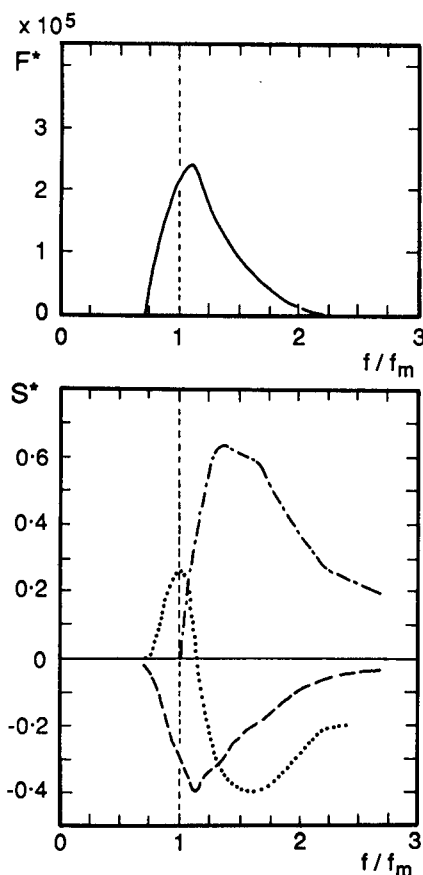
Figure 7   Numerical model output of the wind-wave spectrum and contributions to the wind input (− · −); nonlinear transfer (· · ·); and dissipation (− − −), in the wind direction. (From Komen et al 1984. (Reproduced with the permission of the American Meteorological Society.)

Kolmogorov's universal equilibrium and inertial subrange in describing turbulence spectra, it is not surprising that similar approaches have been made in an attempt to explain the essential characteristics of the surface-wave energy spectrum. The motivation for this work has expanded in recent years with the need to understand active microwave remote sensing data, which are directly affected by small-scale waves of wavelengths of $O(1 \text{ m})$ or less.

Phillips (1958) speculated that, at high frequencies and wavenumbers, saturation due to breaking would occur and that the form of the spectrum could only depend on the frequency σ and gravity g. This led to a frequency spectrum of the form $F(\sigma) = \mathcal{P}g^2\sigma^{-5}$, with $\mathcal{P}$ becoming known as "Phillips constant," and a wavenumber spectrum $F(k) \propto k^{-4}$. During the 1970s, as more measurements of wave spectra became available, it became apparent that $\mathcal{P}$ was not constant. On the basis of laboratory measurements and dimensional analysis Toba (1973) proposed that F should also depend on the wave age c/u_{*a}, which gives

$$F(\sigma) \propto (u_{*a}/c)g^2\sigma^{-5} = u_{*a}g\sigma^{-4}. \tag{8}$$

This result was supported by subsequent laboratory and field data (Kawai et al 1977, Forristall 1981, Donelan et al 1985). Kitaigorodskii (1983) followed Kolmogorov's inertial subrange idea and explicitly considered an equilibrium region in which $I = S_w = D = 0$. As a consequence of this hypothesis he found that

$$F(k) \propto u_{*a}g^{-1/2}k^{-7/2}, \tag{9}$$

$$F(\sigma) \propto u_{*a}g\sigma^{-4}. \tag{10}$$

This frequency spectrum agrees with the more recent observations. Kitaigorodskii's model was quickly followed by an equilibrium model from Phillips (1985). The basis of Phillips' modeling was that the right-hand side of Equation 5 was zero through an equilibrium in which all terms were significant:

$$I + S_w + D = 0, \tag{11}$$

$$I \propto S_w \propto D. \tag{12}$$

Phillips found that the energy spectrum was given by

$$F(\mathbf{k}) = \beta(\cos\theta)^p u_{*a}g^{-1/2}k^{-7/2} \tag{13}$$

and the spectral rate of energy loss was given by

$$\epsilon(\mathbf{k}) = \gamma\beta^3(\cos\theta)^{3p}u_{*a}^3k^{-2}. \tag{14}$$

It may at first seem surprising that the very different hypotheses of Kitaig-orodskii and Phillips should give the same spectral slope of $-7/2$; however, as Phillips pointed out, the slope is determined by the form of I, which is the same in both cases; the assumption of proportionality between the three terms; and dimensional constraints. (This work also provides a more general reminder to fluid dynamicists that the prediction of a spectral slope may be a necessary but not sufficient test of a theory.)

Most recently, Banner (1990b) has synthesized a spectral model based on observations, drawing attention to the importance of the Doppler shifting of shorter waves by longer waves in interpreting frequency spectra. Writing the wavenumber directional spectrum in the form

$$F(k, \theta) = F(k, \theta_{\max})\mathcal{D}(\theta; k), \tag{15}$$

where $F(k, \theta_{\max}) \propto k^{-4}$ and $\mathcal{D}(\theta; k)$ are based on observations (Banner et al 1989), he calculates a frequency spectrum proportional to $u_{*a}\sigma^{-4}$. The differences between Phillips'(1985) and Banner's (1990b) modeling remain to be resolved.

We summarize by noting that our inability to directly measure the spectral distribution of dissipation due to wave breaking is the greatest impediment to the further development of the current generation of wind-wave models. In the absence of these measurements, the local equilibrium hypothesis provides a rational way of estimating the dissipation based on our better knowledge of wind input and weak nonlinear transfers. It is also consistent with a multiple-scale approach in which on short length and time scales the spectrum is in equilibrium, while on longer scales secular changes can occur.

6.   DISSIPATION DUE TO BREAKING

Given the theoretical difficulties associated with the nonlinear breaking, two-phase turbulent flow at free-surfaces, progress in determining the dissipation due to breaking depends on the availability of good experimental data. Although attempts are in progress to infer the dissipation due to breaking in the field, the methods available are indirect. It is most likely that laboratory experiments will continue to provide the most direct and best quality data. The laboratory too has limitations: Most experiments are conducted on quasi-two-dimensional breaking waves in long-wave channels. However, large wave basins are now available that permit the generation of full three-dimensional waves (Lamarre & Melville 1994, Loewen & Melville 1994).

It appears that most breaking waves are unsteady, even in a frame traveling with the underlying wave. Nevertheless, if the time to establish the whitecap

is small compared to its duration then a quasi-steady model may prove useful. Duncan (1981, 1983) generated quasi-steady breaking waves by towing a hydrofoil along a channel. He found that the drag D_b of the whitecap (per unit width) on the underlying flow was given by

$$D_b = \frac{\alpha \rho_w c^4}{g \sin \theta}, \tag{16}$$

where c is the phase speed of the wave and θ is the angle of inclination of the underlying surface to the horizontal. Since the speed of the underlying fluid is approximately c, the work done by the whitecap on the underlying flow, or dissipation per unit length of wave crest ϵ_l, is

$$\epsilon_l = \frac{\alpha \rho_w c^5}{g \sin \theta}. \tag{17}$$

For Duncan's experiments α was in the range 0.0075–0.009 and θ ranged from 6.5 to 14 degrees; this yielded values of $\epsilon_l g / \rho_w c^5$ in the range 0.031–0.066. Duncan's experiments showed that the quasi-steady whitecap evolved into a trailing turbulent surface wake downstream of the wave crest. Cointe & Tulin (1994) developed a simple theoretical model of quasi-steady breaking that showed good agreement with Duncan's measurements.

The quasi-steadiness of Duncan's experiments affords some distinct measurement advantages, but there are aspects of breaking that cannot be addressed with quasi-steady models. For example, the area of the surface (length of the surface in two dimensions) directly broken (turned over or "renewed") by breaking is an important parameter for gas and heat transfer studies. This localization in space and time presents a distinct advantage for experiments on unsteady breaking since fluxes into and out of the breaking region can be measured without the need to confront the difficult job of measuring the details in the breaking region itself. This fact was exploited in a series of experiments by Melville & Rapp (1985), Melville et al (1988), Rapp & Melville (1990), Lamarre & Melville (1991), and Loewen & Melville (1991a). Using dispersive wave packets that focus in the breaking region, Melville & Rapp (1985) measured the wave momentum flux (or energy density) of the packet upstream and downstream of the breaking region, thereby inferring the losses from the wave field due to breaking. Figure 6b shows a plot of the losses against an integral slope parameter for the wave packet upstream. Rapp & Melville (1990) extended these measurements with flow visualization of the volume of fluid mixed down by the turbulence and LDV measurements of the turbulence generated by breaking, finding empirical power laws in time for the evolution of the shape and turbulent kinetic energy of the mixed region that scaled with the prebreaking wave variables. The fact that the turbulence is confined to a local volume of

fluid permitted the correlation of flow visualization of the dyed mixed fluid with the LDV measurements. After only four wave periods from the onset of breaking, less than 10% of the energy lost from the surface waves remained as turbulent kinetic energy. If all the energy (or even a large fraction of it) lost from the wave field initially generates turbulence, then this result implies that the turbulence generated by breaking is highly dissipative. The data showed that for these wave packets of finite bandwidth the energy loss was typically confined to frequencies greater than the center frequency of the packet, with higher frequency losses around the second harmonic band. Visual observation of the wave-gauge time series showed that high-frequency waves were radiated both upstream and downstream of the breaking region. Spectra at low frequency displayed a slight increase downstream of the breaking region. This latter observation would be consistent with the generation of free long waves resulting from the change in the gradients of the radiation stress accompanying breaking. In contrast to the current models of the "dissipation" source term in wind-wave models these results suggest that breaking is not just a sink of wave energy, but may also be a source in some wavenumber-frequency bands.

All of the unsteady breaking experiments cited above displayed dynamical similarity. That is, the variables describing the dissipation and the evolution of the turbulent patch when nondimensionalized by the prebreaking wave variables were a function of an integral measure of the slope of the wave packet. This relationship suggests that we should examine the rate of viscous dissipation in the turbulent patch (Rapp & Melville 1990, Melville 1994). For turbulent flows of sufficiently large Reynolds numbers, the rate of dissipation per unit mass is typically of $O(u^3/l)$, where u and l are integral velocity and length scales respectively. Rapp & Melville's (1990) flow visualization showed that the roughly triangular turbulent region extended to a depth D and a horizontal length comparable to the wavelength λ. If l is comparable to D, the dissipation rate per unit length of crest averaged over the duration of the event ϵ_l is given by

$$\epsilon_l \approx \frac{\rho_w u^3}{l} \frac{l\lambda}{2}. \tag{18}$$

Using the dispersion relationship to express $\lambda(c)$ and the results of Rapp & Melville (1990) gives

$$\frac{\epsilon_l g}{\rho_w c^5} = (3\text{--}16) \times 10^{-3}. \tag{19}$$

Melville (1994), reexamining the data of Loewen & Melville (1991a), found $\epsilon_l g/(\rho_w c^5)$ to be an increasing function of the wave-packet slope and in the range $(4\text{--}12) \times 10^{-3}$. This common scaling of the rate of dissipation for both

the steady and unsteady breaking (cf Equation 17) is simply a result of the dynamical similarity based on the dispersion relationship in each case. The differences arise in the value of the numerical coefficient, which appears to be up to an order of magnitude smaller for the unsteady case—a difference that has yet to be explained.

For the unsteady data cited above, the duration of the breaking was in each case of the order of the wave period; thus the total viscous dissipation of energy per unit length of crest for one breaking event, E_l, is given by $E_l g^2/\rho_w c^6 = O(10^{-2}-10^{-1})$, where the numerical coefficient is at least a function of a measure of the slope of the wave field (Melville 1994) and may also be a function of other dimensionless parameters including moments of the wave spectra.

Based on his equilibrium modeling and Duncan's (1981) data, Phillips (1985) inferred that the contribution to the wave dissipation by breaking events in the speed range c to $c + dc$ was proportional to $u_{a*}^3 c^{-2} dc$ and that $\Lambda(c)$, the length of breaking events in the same speed range per unit area, was proportional to $u_{a*}^3 c^{-7}$. Although measuring the speed of the breaking events is possible (Ding & Farmer 1994a), the dependence of these and other variables on rather large powers of c implies that calculating some of these derived variables from empirical data will be error prone.

Thorpe (1993) has taken a complementary approach and used observations of the incidence of breaking and Duncan's data to infer the total rate of energy loss per unit area of surface as

$$E_w = (3.0 \pm 1.8) \times 10^{-5} \times \rho_w U_{10}^3 (c_b/c_p)^5, \tag{20}$$

where c_b is the characteristic phase speed of the breaking waves, c_p is the phase speed at the peak of the spectrum, and U_{10} is the mean wind speed at 10 m height. Comparison of this expression with mixed-layer data of Oakey & Elliot (1982) led Thorpe to conclude that for that data set $c_b/c_p = 0.25$, with a wavelength ratio of $\lambda_b/\lambda_p = 0.06$. Using the dissipation data from unsteady laboratory experiments and a model of an enhanced dissipation layer in the wave zone, Melville (1994) concluded that the same mixed-layer data implied that c_b/c_p was in the range 0.4–0.63. Despite the uncertainties in both the modeling and the data, it is of interest that the recent acoustical measurements of Ding & Farmer (1994a) show c_b/c_p in the range 0.4–0.75, decreasing as the phase speed at the peak of the spectrum increased. (See Figure 9 below.)

7.   THE WAVE-ZONE BOUNDARY LAYER

Some of the energy lost from the wave field is available as a source of turbulent kinetic energy near the surface, and this leads to the possibility that the

dynamics of the turbulent boundary layer in the wave zone may, as a result of
the direct effects of breaking, be different from that in the classical logarithmic
boundary layer over a rigid surface in which mean shear is the primary source
of turbulence. While mean velocity measurements are the simplest to make in
the laboratory and in the wall region of terrestrial atmospheric boundary layers,
because of instrument motion, direct measurements are difficult to make in the
ocean. Much of the evidence for a distinct wave-zone boundary layer is indirect
and based on measurements of the volumetric dissipation rate per unit mass,
ϵ. Over the past decade a number of measurements in lakes and in the ocean
have detected the presence of a region of enhanced dissipation differing from
$\tilde{\epsilon} \equiv \epsilon \kappa z / u_{*w}^3 = 1$, which applies in the logarithmic law-of-the-wall region.
Here κ is von Karman's constant, z is the depth, and u_{*w} is the friction velocity
in the water. Kitaigorodskii et al (1983), using drag-sphere data from Lake
Ontario, found that $\tilde{\epsilon}$ was up to two orders of magnitude greater than expected
for law-of-the-wall scaling. These experiments were later extended to include
acoustic and LDV measurements, which confirmed that $\tilde{\epsilon}$ was of $O(10–100)$
near the surface, as shown in Figure 8 from Agrawal et al (1992).

Working with the same data Drennan et al (1992) found that the dissipation
decayed as $z^{-\alpha}$, with α in the range 3.0–4.6. Drawing an analogy with grid-
generated turbulence they proposed that the data could be represented by

$$\epsilon = 1.84 u_*^2 c k^{-3} z^{-4}, \tag{21}$$

where c and k are the characteristic phase speed and wavenumber of the waves
supporting the energy flux from the wind. They further suggested that this z^{-4}
dissipation would begin at a depth $z = \beta H_s$, where

$$\beta = 1.2 \left(\frac{U}{c_p} \right)^{0.19} \tag{22}$$

and H_s is the significant wave height.

Gargett (1989) had earlier reported dissipation measurements in the upper
30 m that showed a z^{-4} depth dependence, but did not report any wind depen-
dence in wind speeds up to 12 m s^{-1}. This z^{-4} depth dependence is consistent
with the laboratory grid-mixing measurements of Hopfinger & Toly (1976),
which show the turbulent velocity u decaying as z^{-1} and the integral length
scale l increasing like z away from the source of the turbulence. Thus $\epsilon \propto z^{-4}$,
and the turbulence Reynolds number $R_T \equiv ul/\nu$ is independent of z. This
is equivalent to a constant eddy viscosity. The turbulent kinetic energy in the
decaying grid-generated turbulence results from a balance between dissipation
and turbulent transport, with the energy supplied by the motion of the grid. In
the case of the surface boundary layer, the breaking waves would be the source
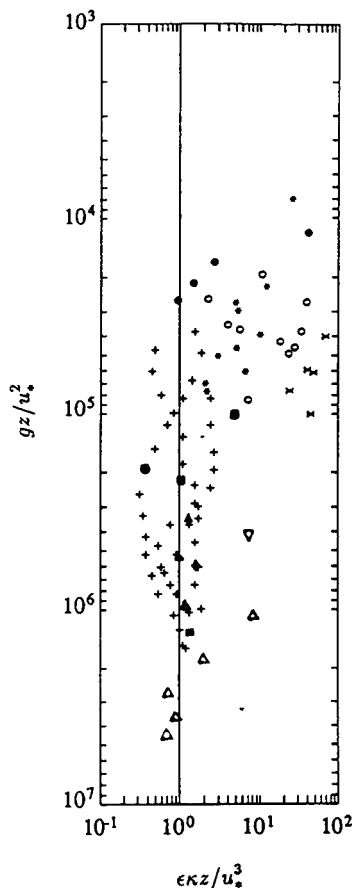
Figure 8 Dissipation in "wall-layer" coordinates $\epsilon \kappa z / u_{*w}^3$ vs zg/u_{*w}^2 measured and collated by Agrawal et al (1992). Included are both lake and ocean data; the vertical line represents the dissipation level in a conventional boundary layer over a rigid surface. [Reprinted with permission from *Nature*. Copyright (1992) Macmillan Magazines Limited.]

of the turbulence. Farther away from the surface, mean-shear-generated turbulent kinetic energy must be added to the balance, leading to the law-of-the-wall scaling and the logarithmic velocity profile for the mean velocity defect $U_s - U$, where U_s is the mean velocity at the surface.

Although the field measurements suggested that breaking was the source of the enhanced dissipation near the surface, none had included any measurements of the incidence of breaking. This motivated Melville (1993, 1994) to determine whether a layer of enhanced dissipation near the surface was consistent with the modeling of dissipation due to breaking in wind-wave models and laboratory measurements of breaking and mixing. Using Phillips' (1985) equilibrium model and the data of Rapp & Melville (1990), Melville (1993, 1994) concluded

that a well-mixed surface layer should exist to a depth of the order of the breaking wave height with volumetric dissipation rates one to two orders of magnitude greater than the law-of-the-wall result, consistent with the data of Agrawal et al (1992).

The most complete attempt so far to incorporate these ideas into a model was made by Craig & Banner (1994), who used a standard scheme to close the mean momentum and turbulent kinetic energy equations for the boundary layer in a rotating fluid. This scheme uses eddy viscosities to represent the effects of the Reynolds stresses and turbulent transport terms, and it employs an integral length scale proportional to the distance from the boundary. Craig & Banner considered separately the balance between shear generation and dissipation and between turbulent transport and dissipation. In the latter case they found that ϵ was given by

$$\epsilon = 2.4u_{*w}^3 a z_0^n (z_0 - z)^{-n-1}, \tag{23}$$

with $n = 2.4$. Thus $\epsilon \propto z^{-3.4}$, within the range reported by Drennan et al (1992) and close to the z^{-3} found in the field data of Anis & Moum (1992). For this turbulent kinetic energy balance, $U_s - U$ varied as $z^{0.8}$, close to a constant mean shear that would be expected if the eddy viscosity were constant. However, in a comparison with the data of Agrawal et al (1992), the full numerical model, including both shear generation and turbulent transport, gave a somewhat slower decay of dissipation with depth.

Very recently two papers have appeared from the group that published Agrawal et al (1992) and Drennan et al (1992). The first (Terray et al 1995) carefully edited the earlier lake data to remove conditions that may have led to platform interference and other errors. They now find a slower decay of dissipation with depth so that

$$\frac{\epsilon H_s}{u_{*w}^2 \bar{c}} = 0.3(z/H_s)^{-2}, \tag{24}$$

where $\bar{c}$ is an effective phase speed for wind input such that the energy flux from wind to waves is $\rho_w u_{*w}^2 \bar{c}$. It is of interest to note that $\bar{c}/c_p$ was roughly 0.1 near full development, but was in the range 0.35 to 0.75 for inverse wave age u_{*a}/c_p greater than 0.075, the range for which the dissipation data were analyzed. This may be compared with the normalized breaking wave speeds, c_b/c_p, inferred by Melville (1994) and measured by Ding & Farmer (1994a). (See Section 6.) Drennan et al (1995) report on ship-based ocean dissipation measurements during the Surface WAves Dynamics Experiment (SWADE) and find good agreement with the lake data and the z^{-2} decay. These are difficult measurements to make and there is considerable scatter in the combined data

sets (up to two orders of magnitude in the dimensionless dissipation), so firm conclusions about vertical gradients in dissipation can not be made at this time. What is clear is that much work needs to be done to measure and model turbulence in the surface wave zone.

Left unresolved by the turbulence closure modeling is the problem of estimating the roughness length z_0: Craig & Banner use values in the range 0.1–8 m to obtain rough agreement with the field measurements of ϵ. In these boundary layer models, $z = z_0$ gives the position of the virtual surface at which $U = U_s$. If turbulence generation in the wave zone is dominated by wave breaking, then it will be intermittent at the larger scales of wave breaking and perhaps less so for microscale (decimeter) breaking. Typical rates of visible breaking at a point are of $O(0.01–0.1)$ breaking waves per wave, based on the period of waves at the peak of the spectrum (see Holthuisen & Herbers 1986). If breaking is dominated by waves at frequencies greater than the peak of the spectrum, then the laboratory evidence suggests that the initial penetration of turbulence will be to depths of the order of the breaking wave height. This turbulence will then be transported by the turbulence itself, the orbital motion of the larger longer waves, and perhaps by Langmuir circulations. All of these effects may serve to mix the momentum and determine the position of the virtual surface (or z_0). Indeed, there may in fact be at least two virtual origins: one for the constant-shear region (transport/dissipation balance) and one for the logarithmic layer (shear generation/dissipation balance). Furthermore, breaking is not the only possible source of turbulence in the surface layers with thermal convection, Langmuir circulations, and even rainfall also contributing. Because the analogy with grid mixing may also apply to these sources, it may prove difficult, on the basis of the scaling of dissipation by analogy to grid mixing, to reconcile field measurements of z_0 with simple models. Scaling and modeling of z_0 in the atmospheric marine boundary layer remains an area of active research.

8.   GAS TRANSFER

Public debate has heightened awareness of the importance of the oceans in modulating secular changes in climate. Perhaps nothing has attracted as much attention as the influence of the increase in greenhouse gases on global warming. Quantitative estimates of the role of the oceans in taking up increases in CO_2 are based in part on global budgets that involve considerable uncertainty. As Baggeroer & Munk (1992) have recently observed in their status report on acoustic monitoring of ocean warming, "... all we know for sure is that the oceans are an important sink of heat, and CO_2, and of ignorance."

For moderately soluble gases such as CO_2 and O_2, the transfer across the air-sea interface at lower wind speeds is controlled by the aqueous boundary

layer (Jähne 1990) and is parameterized in terms of a gas transfer velocity k, where the molar flux of gas across the interface is given by $j = k\Delta c$ and Δc is the difference between the saturation and bulk concentration of the dissolved gas. For low wind speeds, wind-wave laboratory studies have shown that

$$k = \alpha Sc^{-0.5}u_{*w} \tag{25}$$

(Jähne 1990, Khoo & Sonin 1992), where $Sc = \nu/\kappa$ is the Schmidt number, the ratio of the kinematic viscosity of the fluid to the diffusion coefficient of the dissolved gas, and the numerical coefficient α is of $O(10^{-1})$. At higher wind speeds, above 10–12 m s^{-1} say, there is a relatively sharp increase in α (an approximate doubling), with higher wind speeds giving a correspondingly higher transfer velocity (Broeker & Siems 1984, Merlivat & Memery 1983, Liss & Merlivat 1986). This increase in the transfer velocity has been attributed to the onset of breaking and bubble entrainment and is qualitatively consistent with the sonar measurements of bubble clouds and modeling by Thorpe (1982), who concluded that the gas flux from the bubbles may dominate the air-water gas flux at wind speeds above 12 m s^{-1}.

However, recent experiments by Khoo & Sonin (1992) in which the turbulence is induced by agitation from below with no breaking nor air entrainment show a similar break and enhancement of the gas transfer. Notwithstanding this uncertainty regarding the mechanism leading to enhanced gas transfer at higher wind speeds, Jähne (1990) has demonstrated that the addition of a mechanically generated breaking wave to a wind-generated wave field in the laboratory can enhance the gas transfer by a factor of two.

Parameterization and modeling of air-sea gas transfer processes have depended to a great extent on laboratory studies, which may not faithfully represent the full complexity of the wind-driven sea surface. The opportunities for field studies of gas transfer have improved recently with the development of continuous onboard analytical techniques and relatively rapid-response dissolved-gas sensors that can be deployed in the field for extended periods. Watson et al (1991) used a dual-tracer technique in which two inert gaseous tracers (SF$_6$ and ^{3}He) were released into a shallow sea and concentrations were subsequently measured for up to ten days. Their measurements were consistent with Liss & Merlivat's (1986) parameterization, including enhanced gas transfer at higher wind speeds. In a recent field experiment in the Middle Atlantic Bight, Wallace & Wirick (1992) deployed a pair of dissolved oxygen sensors at two depths (19 m and 34 m) for a period of four months. They found that the time series of dissolved oxygen were distinguished by sudden large increases associated with surface-wave activity, followed by longer periods of degassing between storms (Figure 9). Their data supported the conclusion that the gas invades rapidly to supersaturation as a result of pressurization of bubbles entrained to depths of
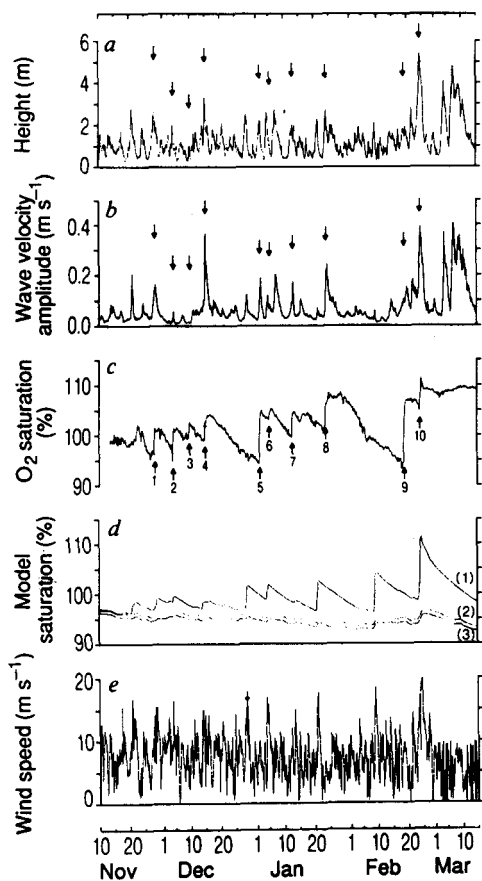
Figure 9   Field measurements of dissolved oxygen and other environmental variables, including wave height, orbital velocity, and wind speed. Note the rapid increase in the dissolved gas with storm events indicated in the orbital velocity time series and the slower relaxation back to lower levels. The model results cited in the text are denoted by the numerals 1–3. (From Wallace & Wirick 1992.) [Reprinted with permission from *Nature*. Copyright (1992) Macmillan Magazines Limited.]

several meters, but evades more slowly via transport across the air-sea interface. They compared their measurements with the semi-empirical models of Thorpe (1984) and Spitzer & Jenkins (1989) (both of which included bubble transport) and a thin-film model (which excluded bubble transport).[3] They concluded that Thorpe's model gave the best agreement with the measurements, but because it was forced by wind rather than waves, some discrepancies arose. In a more detailed but shorter experiment, Farmer et al (1993) measured gas tension (the sum of the partial pressures of the dissolved gases) at a number of depths down to 20 m in a single storm event. Comparing their results with the direct surface transfer model of Liss (1988), and models of Thorpe (1984) and Woolf & Thorpe (1991), they concluded that a time-dependent correction factor of up to 4 was required to give agreement between Woolf & Thorpe's (1991) model and their gas tension data in the surface layer. This discrepancy was attributed to an underestimation of the transfer of weakly soluble gases during periods of bubble penetration associated with breaking.

The role of bubbles in air-sea gas exchange is poorly understood, but two recent modeling studies have drawn attention to the role of larger bubbles. The details of this type of modeling, which combines single bubble dynamics and physical chemistry with input from laboratory and field data, is beyond the scope of this review, but it is worth mentioning some of the more important results. Keeling (1993) concluded that bubble-mediated gas transfer depends critically on the production rates of bubbles greater than approximately 1 mm in diameter. He suggested that by neglecting the larger bubbles Woolf & Thorpe (1991) may underestimate substantially the role of bubbles in gas exchange. Keeling also found that the enhanced gas transfer at higher wind speeds as parameterized by Liss & Merlivat (1986) was approximately reproduced by his modeling, suggesting that most of the enhancement may be explained by bubble entrainment, which would be more important for less soluble gases. In a related study, Woolf (1993) reaches similar conclusions, and like Keeling stated that confident prediction of bubble-mediated gas transfer remains difficult.

One of the integral constraints on bubble-mediated gas transfer is the total volume of gas entrained by breaking waves. It is commonly assumed that this quantity is related to whitecap coverage (i.e. the fraction of the sea surface covered by foam (Monahan & McNiocaill 1986) or to a fraction of the whitecap coverage associated with actively breaking waves. Breaking waves may entrain a volume of air that evolves into a bubble size distribution. In the actively breaking waves the local volume fraction of air may range from $O(0.1)$ to $O(1)$, but this rapidly decreases over a time comparable to the wave period as the larger bubbles rise back to the surface (Lamarre & Melville 1991). The smaller

---

[3] Note that these three model results are denoted by 1, 2, and 3, respectively, in Figure 9.

bubbles are entrained by the turbulent flow and mix down to greater depths, with the smallest bubbles faithfully following the flow. Thus the bubble clouds near the surface may be crudely separated into short-lived, high-void-fraction plumes of large bubbles close to the surface [$O(1$ m) depth] embedded in a more slowly varying, low-void-fraction background field of smaller bubbles extending to greater depths [$O(10$ m)]. This background comprises the dispersed remnants of earlier bubble injection events. For gas transfer studies one would like to know the size distribution of bubbles entrained at the surface and be able to measure and predict its evolution. Several attempts have been made in this direction (e.g. Thorpe 1982), but given all the uncertainties in specifying the velocity field and the initial bubble size distribution, we can not be confident of their predictive capabilities at this time.

Measurements of bubble plumes using upward-looking sonars (Thorpe 1982, 1992; Vagle & Farmer 1992) at acoustic frequencies of $O(100$ kHz) are excellent for imaging the small-bubble clouds, but if Keeling (1993) and Woolf (1993) are correct then it is the larger bubbles much closer to the surface that may play the dominant role for more soluble trace gases, especially carbon dioxide. Impediments to improved modeling of bubble transport include uncertainties about initial distributions of bubble sizes and subsequent breakup, turbulent transport, and surface chemistry and contamination. A recent detailed review of this important and fascinating subject is given by Thorpe (1992).

The enhancement of gas transfer by breaking is due to not only bubble entrainment but also to the local increase in turbulent intensity and dissipation accompanying breaking. Kitaigorodskii (1984) has modeled the influence of patches of enhanced turbulence caused by breaking. He finds that the transfer velocity k is proportional to $Sc^{-1/2}[\nu\epsilon(0)]^{1/4}$, where $\epsilon(0)$ is the dissipation of turbulent kinetic energy near the surface.[4] This expression had been derived earlier in a different context by Lamont & Scott (1970) and is in agreement with experiments of Dickey et al (1984) in a grid-mixing tank. The scaling of k is also consistent with mass diffusion across a layer of the thickness of the Batchelor (1959) scale $\delta_B = Sc^{-1/2}\eta$ for $Sc \gg 1$, where η is the Kolmogorov microscale. The Schmidt number for gases in seawater is of $O(10^3)$, and the Batchelor scale corresponds to the beginning of the viscous-diffusive subrange in the spectrum of the concentration fluctuations. It is of interest to determine the effects of the enhanced dissipation discussed above in the light of Kitaigorodskii's result. From our estimates of Section 7 we expect an enhancement of the dissipation by a factor of $O(10-100)$. According to Kitaigorodskii this would lead to an increase in the transfer velocity by a factor of 2–4, which is

---

[4]Note that Kitaigorodskii used the Prandtl number to denote the ratio of the diffusion of momentum to mass. This number is usually reserved for heat transfer.

in the range of enhancement caused by breaking found by Jähne (1990) in the laboratory and is comparable to the correction factor of Farmer et al (1993), which was attributed to bubble effects. Thus, if bubble effects, which depend on solubility, are to be unambiguously separated from the effects of enhanced mixing or dissipation due to breaking, then the fluxes of gases of different solubilities will have to be measured simultaneously.

9. THE ACOUSTICS OF BREAKING WAVES

Until recently, ambient sound in the audio range (20–20,000 Hz) in the ocean was broadly classified as being due to ocean turbulence (<100 Hz), shipping traffic (<1 kHz), and "wind" noise (100–20,000 Hz) and was represented by smooth empirical spectra (Wenz 1962). Commercial oceanographic instrumentation even exploited the correlation between ambient noise and wind speed (see Vagle et al 1990). While it was recognized that much of the wind noise was in fact due to breaking, it is only in the last ten years that attention has focused more directly, and in a quantitative fashion, on the relationship between ambient noise at the ocean surface and surface-wave breaking. The beginnings of much of this work are summarized in the proceedings of a conference that brought together acousticians and hydrodynamicists in Lerici in 1987 (Kerman 1988). By that time field measurements had shown that discrete acoustic events could be identified with breaking (Farmer & Vagle 1988), and there was considerable speculation about the source of the sound. Sources of sound associated with the entrainment of air are almost certainly the dominant source of sea-surface sound. After entrainment the volume of air is broken up into smaller and smaller bubbles. At the time of its generation a bubble is not in its equilibrium shape or volume, and as it relaxes to this equilibrium spherical shape it oscillates in its axisymmetric ("breathing") mode. This volume mode of oscillation is the most efficient for the radiation of sound and has a frequency

$$\omega^2 = 3\gamma P / \rho_w r^2, \tag{26}$$

where γ is the ratio of the specific heats of the gas, P is the equilibrium pressure, ρ_w is the density of the liquid (water), and r is the equilibrium bubble radius (Minnaert 1933. Leighton 1994). For a bubble of 1-mm radius in water at atmospheric pressure, the resonant frequency is approximately 3.26 kHz. Banner & Cato (1988) presented a video recording of the sound generated in this fashion by bubbles pinching off in a quasi-steady spilling breaker. In a series of laboratory experiments, Medwin and his colleagues (Medwin & Beaky 1989, Medwin & Daniel 1990) have shown that bubble resonance is the dominant source of sound at frequencies greater than approximately 400–500 Hz for gently breaking waves.
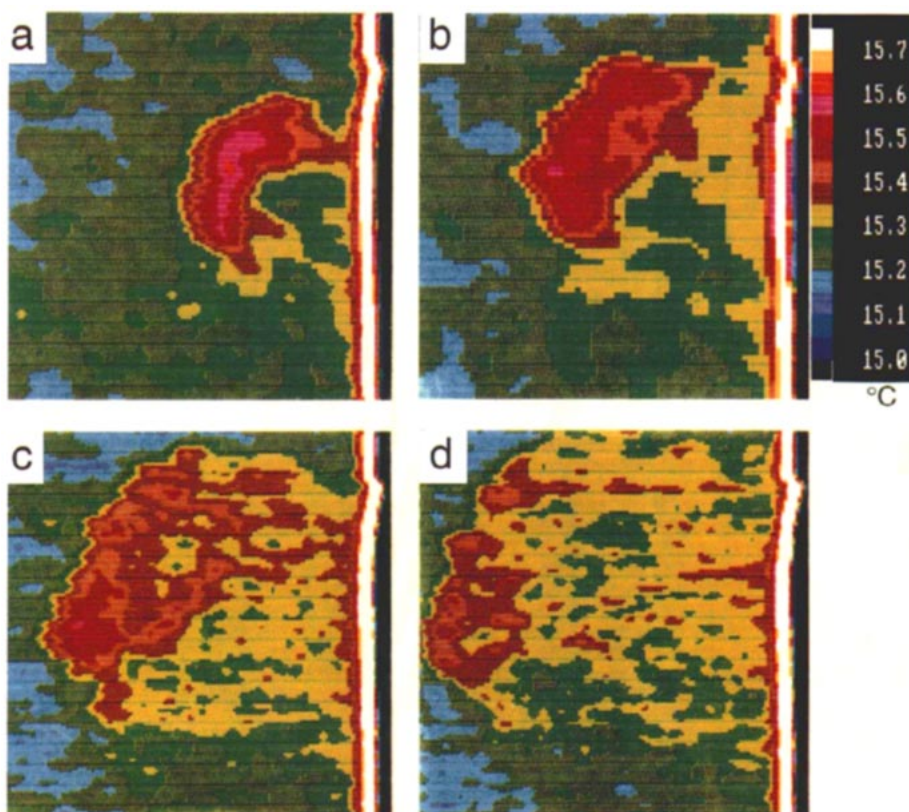
Figure 5 An infrared image of a breaking wave disrupting the cooler surface layer and mixing up warmer water from below. Note the evolution of the turbulent patch and the range of scales in the temperature field. The images represent a patch of surface 5 m × 5 m and are taken 0.25 s apart. (From Jessup 1995.)

It is of interest to determine whether the sound generated by breaking can be used to do more than just identify breaking events. Preliminary experiments showed that for frequencies greater than 500 Hz the sound radiated by breaking waves in the laboratory correlated with the energy dissipated (Melville et al 1988). If this correlation were to apply to the field, it would offer an efficient way of monitoring surface-wave dissipation, a difficult measurement to make directly. These preliminary results were confirmed in more extensive laboratory measurements (Loewen & Melville 1991a) that showed that of the order of 10^{-8} of the mechanical energy dissipated was radiated as sound. (This ratio can be thought of as an "acoustic efficiency.") Subsequently, field measurements of Kennedy (1992, 1993) showed approximate scaling of the acoustic source spectrum with wave dissipation estimates based on Phillips' (1985) model and efficiencies comparable to those measured in the laboratory. Simple semi-empirical modeling (Loewen & Melville 1991b) showed that, for gently spilling waves, measurements of the sound radiated above approximately 400 Hz (Medwin & Beaky 1989, Medwin & Daniel 1990) could be reproduced with a simple acoustic dipole model of bubbles entrained at the surface. Implicit in this result is the fact that the sound radiated is proportional to the volume of air entrained.

Although these results are encouraging for gently spilling waves they do not account for the air entrainment and acoustics of more energetically breaking waves in which large volumes of air are entrained. In these cases it is more useful to consider the whitecap as a continuum described by its geometry and void-fraction field, rather than a collection of discrete bubbles. By measuring the electrical conductivity of the air-water mixture in the whitecap, Lamarre & Melville (1991) were able to infer the void fraction field and hence the evolution of the bubble cloud in unsteady breaking waves. They found that all of the lower-order moments of the void-fraction field evolved as simple exponential or power-law functions in time (Figure 10). These data are of interest for acoustic and gas transfer studies, but the most important dynamical result of this work was to show that the energy expended in entraining the air against buoyancy forces could account for up to 50% of the total surface-wave energy dissipated. This result serves to support the earlier empirical correlation between energy dissipation and sound radiation. Subsequent field work using similar conductivity probes showed that the large void fractions measured in the laboratory [$O(10\%)$] were also present in the field (Lamarre & Melville 1992).

Bubble clouds may also oscillate as a whole in what are called "collective oscillations." The possibility that such oscillations could occur in bubble clouds entrained by breaking waves had been considered by Prosperetti (1988) and by
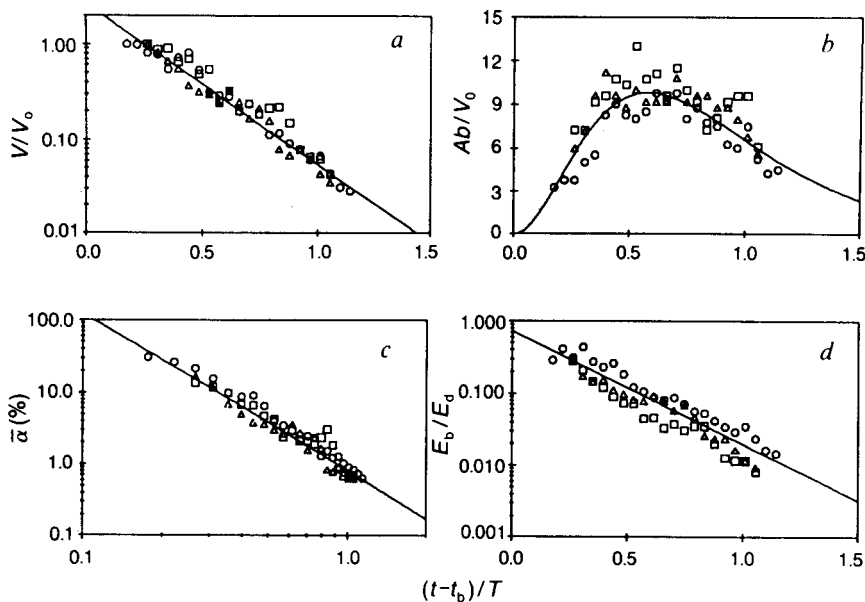
Figure 10   Moments of the void fraction field as a function of normalized time measured under unsteady breaking waves in the laboratory. V/V_0: normalized total volume of air; Ab/V_0: normalized area of the bubble cloud, where b is the breadth of the channel; $\bar{\alpha}$: mean void fraction in percent; E_b/E_d: ratio of the potential energy of the bubble cloud to the total energy dissipated in breaking. [From Lamarre & Melville 1991. (Reprinted with permission from *Nature*. Copyright (1991) Macmillan Magazines Limited.)]

Carey & Browning (1988) as a source of low-frequency sound (<500 Hz) at the ocean surface, although the phenomenon was earlier recognized in cavitation studies (d'Agostino & Brennan 1983). The lowest mode of oscillation of a spherical bubble cloud has a frequency

$$\Omega = \frac{1}{R}\left(\frac{3\gamma P}{\rho_w \bar{\alpha}}\right)^{1/2}, \tag{27}$$

where R is the radius of the cloud, γ is the ratio of the specific heats, P is the equilibrium pressure inside the individual bubbles comprising the cloud, and $\bar{\alpha}$ is the mean void fraction. If isothermal conditions apply, $\gamma = 1$. For example, if $R_0 = 0.3$ m, $\bar{\alpha} = 0.1$, and $P = 101$ kPa, then $\Omega = 30 \times 2\pi$ rad s^{-1}. Hollet (1989) and Farmer & Vagle (1988) had shown in the field that low-frequency sound accompanies wave breaking. Direct evidence that collective oscillations may be the source of low-frequency sound in breaking waves was provided

in two complementary sets of laboratory measurements. Lamarre & Melville (1994) measured the void fraction in both two- and three-dimensional breaking waves. These data were then used to predict the eigenfrequencies of the collective oscillations of the bubble clouds and compared with low-frequency sound measurements by Loewen & Melville (1994). For spilling breaking (with little air entrainment), the sound radiated below approximately 500 Hz did not vary with the strength of the break; however, on the transition to plunging breaking, the low-frequency sound was clearly a function of the strength of the break, and spectral peaks could be identified. Comparisons between measured and predicted frequencies of collective oscillations were very good. Most recently Oguz (1994) has proposed a model of ambient sound in the ocean based on individual bubble resonances at higher frequencies coupled to collective oscillations at lower frequencies.

In recent field measurements Ding & Farmer (1994a,b) have used a small hydrophone array on a drifting buoy to identify, track, and quantify breaking. Using travel-time and correlation techniques they have been able to measure the location and velocity of the breaking events and relate them to the surface-wave properties (Figure 11). Of particular interest is the characterization of the breaking in terms of the velocity of the events (cf Phillips 1985) and the support for the prospect of using acoustics to infer dissipation (cf Melville et al 1988, Loewen & Melville 1991a). Taken together this may lead to indirect information about the wavenumber dependence of dissipation due to breaking. Felizardo & Melville (1995) have recently shown a good correlation between field measurements of ambient sound and the dissipation models of Hasselmann and Phillips.

The success of relatively simple acoustic models for predicting parameters describing the sound radiated by breaking waves is reason for confidence that ambient sound may be a useful tool for learning more about air-sea fluxes. For example, it is relatively simple to demonstrate that plausible approximations may lead to an order of magnitude estimate of the total volume of air entrained. The frequency f_r of the lowest acoustic mode of a cloud of bubbles that is collectively oscillating is given by $f_r = f_r(c_m, a, s_i)$, where c_m is the low frequency sound speed in the mixture, a is a characteristic scale of the cloud, and s_i are dimensionless parameters describing the shape of the cloud. From dimensional reasoning the dimensionless frequency $\tilde{f}_r \equiv f_r a / c_m$ is given by

$$\tilde{f}_r = AS(s_i), \tag{28}$$

where A is a constant. Now

$$c_m = \left[\frac{p}{\rho_w \alpha (1 - \alpha)} \right]^{1/2}, \tag{29}$$

where p is the pressure, α is the void-fraction, and the volume of air entrained $V = \alpha a^3$, which defines a. Therefore,

$$V = \left[\frac{ASp^{1/2}}{\rho_w^{1/2}} \right]^3 G(\alpha) f_r^{-3}, \qquad (30)$$

where $G(\alpha) = [\alpha(1 - \alpha)^3]^{-1/2}$. Since p and ρ_w are effectively constant near the surface, if the bubble clouds are geometrically similar (cf Lamarre & Melville 1991), then S is a constant. If f_r is measured, then V is known to within the value of the function $G(\alpha)$, which varies within a factor of $O(1)$ for $0.01 < \alpha < 0.5$, the typical range of void fractions found in the laboratory
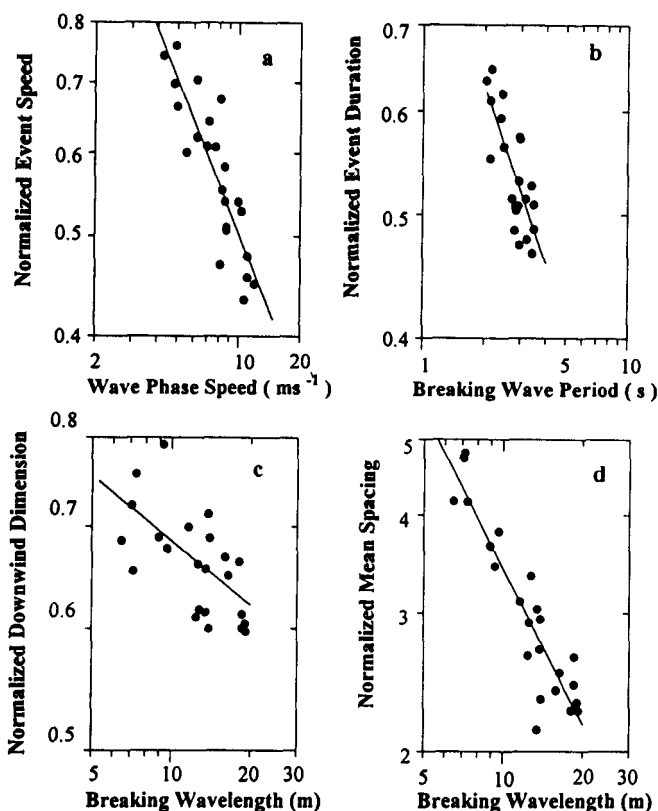
Figure 11 Kinematic and geometric properties of breaking waves normalized by the abscissa variable measured acoustically in the ocean by Ding & Farmer (1994a) using a small drifting hydrophone array. (Reproduced with the permission of the American Meteorological Society.)

for bubble clouds in collective oscillation. In other words, the measurement of just the frequency of the lowest mode of collective oscillation of a bubble cloud may lead to an order of magnitude estimate of the total volume of air entrained. Additional measurements of c_m or a (cf Lamarre & Melville 1994) would lead to much more precise estimates of the total air entrained by whitecaps, which are important data for gas transfer studies.

10. EPILOGUE

The subject of this review is an area of rapid progress with implications for fluid mechanics, oceanography, and meteorology.

It should be clear that just identifying breaking in a random wave field is a difficult problem made more difficult by the fact that there may be closely related wave phenomena associated with steep but unbroken waves. Important recent work by Longuet-Higgins (1992, 1994, 1995) on parasitic capillary waves and bores has drawn attention to the generation of vorticity in regions of large surface curvature and its transport into the interior of the fluid, leading to a turbulent wake. The generation of parasitic capillaries leads to enhanced dissipation of the longer waves on which they ride. Longuet-Higgins (1992) has suggested that the shed vorticity may be concentrated in a roller at the crest of the wave. Thus it may be difficult to distinguish between gently breaking waves and steep waves generating parasitic capillaries.

The generation of vorticity in regions of large curvature of the surface is due to the baroclinic generation term, with the transport of vorticity away from the immediate neighbourhood of the surface caused by viscosity (Wu 1995). Irrotational flows that evolve to breaking and entrain a volume of air may also generate a finite circulation when the surface closes on itself and the fluid is no longer simply connected. This mechanism of vorticity generation has been discussed at various meetings and seminars over the years but as far as I am aware its first brief mention in print is in Thorpe (1985) and more graphically in Hornung et al (1995) in the context of the generation of vorticity across a hydraulic jump. No detailed quantitative study has been undertaken to explore the implications of this phenomenon. Once the entrained air breaks up into a cloud of bubbles the inhomogeneous mixture will also be subject to baroclinic generation of vorticity. The generation of a large coherent vortex by unsteady breaking is presented in the data of Rapp & Melville (1990). [See also Miller (1976) for corresponding images of vortices in shallow water breaking waves.] Recent particle imaging velocimetry (PIV) by Lin & Rockwell (1994, 1995) shows the velocity and vorticity field in a quasi-steady breaking wave. The numerous PIV studies of breaking that are presently underway should lead to a much better understanding of the vorticity generated by breaking waves.

The much greater heat capacity of water compared to air implies that even shallow surface layers of water that are at temperatures significantly different from water slightly deeper in the ocean mixed layer may be important for air-sea heat transfer. For example, in the "warm pool" in the western equatorial Pacific Ocean, in low winds surface layers a few meters deep may be as much as $3°K$ warmer than the water below, and similar but less dramatic temperature differences may apply in other regions. If the turbulence in the surface boundary layer is dominated by breaking at higher winds, then we can anticipate that in such conditions breaking will play a significant role in heat transfer in the upper ocean. (See Farmer & Gemmrich 1995.) This also has important implications for remote sensing of the sea-surface temperature as is made clear in Figure 5.

Literature Cited

Agrawal YC, Terray EA, Donelan MA, Hwang PA, Williams AJ III, et al. 1992. Enhanced dissipation of kinetic energy beneath breaking waves. *Nature* 359:219–20

Anis A, Moum JN. 1992. The superadiabatic surface layer of the ocean during convection. *J. Phys. Oceanogr.* 22:1221–27

Baggeroer A, Munk W. 1992. The Heard Island Feasibility Test. *Phys. Today* 45:22–30

Banner ML. 1990a. The influence of wave breaking on the surface pressure distribution in wind wave interactions. *J. Fluid Mech.* 211:463–95

Banner ML. 1990b. Equilibrium spectra of wind waves. *J. Phys. Oceanogr.* 20:966–84

Banner ML, Cato DH. 1988. Physical mechanisms of noise generation by breaking waves—a laboratory study. See Kerman

1988, pp. 429–36

Banner ML, Fooks EH. 1985. On the microwave reflectivity of small-scale breaking water waves. *Proc. R. Soc. London Ser. A* 399:93–109

Banner ML, Jones ISF, Trinder JC. 1989. Wavenumber spectra of short gravity waves. *J. Fluid Mech.* 198:321–44

Banner ML, Melville WK. 1976. On the separation of air flow over water waves. *J. Fluid Mech.* 77:825–42

Banner ML, Peregrine DH. 1993. Wave breaking in deep water. *Annu. Rev. Fluid Mech.* 25:373–97

Banner ML, Phillips OM. 1974. On the incipient breaking of small scale waves. *J. Fluid Mech.* 65:647–56

Batchelor GK. 1959. Small-scale variation of convected quantities like temperature in turbulent fluid, Part 1. General discussion and the case of small conductivity. *J. Fluid Mech.* 5:113–33

Benjamin TB, Feir JE. 1967. The disintegration of wave trains in deep water. Part 1, Theory. *J. Fluid Mech.* 27:417–30

Bonmarin PJ. 1989. Geometric properties of deep-water breaking waves. *J. Fluid Mech.* 209:405–33

Broecker HC, Siems W. 1984. The role of bubbles for gas transfer from water to air at higher windspeeds. In *Gas Transfer at Water Surfaces*, ed. W Brutsaert, GH Jirka, pp. 229–36. Dordrecht: Reidel. 639 pp.

Carey WM, Browning DG. 1988. Low frequency ocean ambient noise: measurements and theory. See Kerman 1988, pp. 361–76

Cointe R, Tulin MP. 1994. A theory of steady breakers. *J. Fluid Mech.* 276:1–20

Craig PD, Banner ML. 1994. Modeling wave-enhanced turbulence in the ocean surface layer. *J. Phys. Oceanogr.* 24:2546–59

Crowther PA, Hansla A. 1993. The lifetimes, velocities and probable origin of sonic and ultrasonic noise sources on the sea surface. In *Natural Physical Sources of Underwater Sound*, ed. BR Kerman, pp. 379–92. Dordrecht: Kluwer. 750 pp.

d'Agostino L, Brennan CE. 1983. On the acoustical dynamics of bubble clouds. In *Cavitation and Multiphase Flow Forum—1983*, ed. JW Hoyt, pp. 72–75. New York: ASME. 96 pp.

Dickey TD, Hartman B, Hammond D, Hurst E. 1984. A laboratory technique for investigating the relationship between gas transfer and fluid turbulence. In *Gas Tranfer at Water Surfaces*, ed. W Brutsaert, GH Jirka, pp. 93–100. Dordrecht: Reidel. 639 pp.

Ding L, Farmer DM. 1994a. Observations of breaking surface wave statistics. *J. Phys. Oceanogr.* 24:1368–87

Ding L, Farmer DM. 1994b. On the dipole acoustic source level of breaking waves. *J. Acous. Soc. Am.* 96:3036–44

Dold JW, Peregrine DH. 1986. Water-wave modulation. *Proc. 20th Conf. Coastal Eng., Taipei*, 1:163–75. Minneapolis: ASCE

Dommermuth DG, Yue DKP, Rapp RJ, Chan E-S, Melville WK. 1987. Deep-water breaking waves: a comparison between potential theory and experiments. *J. Fluid Mech.* 89:432–42

Donelan M, Longuet-Higgins MS, Turner JS. 1972. Periodicity in whitecaps. *Nature* 239:449–51

Donelan MA, Hamilton J, Hui WH. 1985. Directional spectra of wind-generated waves. *Phil. Trans. R. Soc. London Ser. A* 315:509–62

Drennan WM, Kahma KK, Terray EA, Donelan MA, Kitaigorodskii SA. 1992. Observations of the enhancement of kinetic energy dissipation beneath breaking wind waves. In *Breaking Waves: IUTAM Symposium Sydney, Australia 1991*, ed. ML Banner, RHJ Grimshaw, pp. 95–102. Berlin/Heidelberg: Springer-Verlag. 387 pp.

Duncan JH. 1981. An experimental investigation of breaking waves produced by a towed hydrofoil. *Proc. R. Soc. London Ser. A* 377:331–48

Duncan JH. 1983. The breaking and non-breaking wave resistance of a two-dimensional hydrofoil. *J. Fluid Mech.* 126:507–20

Duncan JH, Philomin V, Behres M, Kimmel J. 1994a. The formation of spilling breaking water waves. *Phys. Fluids.* 6:2558–60

Duncan JH, Philomin V, Qiao H, Kimmel J. 1994b. The formation of a spilling breaker. *Phys. Fluids* 6:S2

Farmer DM, Gemmrich JR. 1995. Measurements of temperature fluctuations in breaking surface waves. *J. Phys. Oceanogr.* In press

Farmer DM, McNeil CL, Johnson BD. 1993. Evidence for the importance of bubbles in increasing air-sea gas flux. *Nature* 361:620–23

Farmer DM, Vagle S. 1988. On the determination of breaking wave distributions using ambient sound. *J. Geophys. Res.* 93:3591–600

Felizardo FC, Melville WK. 1995. Correlations between ambient noise and the ocean surface wave field. *J. Phys. Oceanogr.* 25:513–32

Forristall GZ. 1981. Measurement of a saturation range in ocean wave spectra. *J. Geophys. Res.* 86:8075–84

Frasier SJ, Liu Y, Moller D, McIntosh RE, Mead JB. 1995. Directional ocean wave measurements in a coastal setting using a focused array imaging radar. *IEEE Trans. Geosci. Rem. Sens.* 33:428–40

Gargett AE. 1989. Ocean turbulence. *Annu. Rev.*

Fluid Mech. 21:419–51

Gill AE. 1982. *Atmosphere-Ocean Dynamics.* London: Academic. 662 pp.

Hasselmann K. 1962. On the nonlinear energy transfer in a gravity-wave spectrum. Part 1: General theory. *J. Fluid Mech.* 12:481–500

Hasselmann K. 1974. On the spectral dissipation of ocean waves due to white capping. *Boundary-Layer Meteorol.* 6:107–27

Hollet R. 1989. Underwater sound from white caps at sea. *J. Acous. Soc. Am.* 85(S1): S145

Holthuijsen LH, Herbers THC. 1986. Statistics of breaking waves observed as whitecaps in the open sea. *J. Phys. Oceanogr.* 16:290–97

Hopfinger EJ, Toly J-A. 1976. Spatially decaying turbulence and its relation to mixing across density interfaces. *J. Fluid Mech.* 78:155–75

Hornung HG, Willert C, Turner S. 1995. The flow field downstream of a hydraulic jump. *J. Fluid Mech.* 287:299–316

Hsu CT, Hsu EY, Street RL. 1981. On the structure of turbulent flow over a progessive water wave: theory and experiment in a transformed, wave following co-ordinate system. *J. Fluid Mech.* 105:87–117

Hsu CT, Wu HW, Hsu EY, Street RL. 1982. Momentum and energy transfer in wind generation of waves. *J. Phys. Oceanogr.* 12:929–51

Jähne B. 1990. New experimental results on the parameters influencing air-sea gas exchange. In *Proc. Air-Water Mass Transfer: Second Int. Symp,* ed. SC Wilhelms, JS Gulliver, pp. 582–92. Minneapolis: ASCE

Jessup AT. 1995. The infrared signature of breaking waves. In *Proc. Symp. on Air-Sea Interaction, Marseille, France 1993,* ed. MA Donelan, WJ Plant, WH Hui. Toronto: Univ. Toronto Press

Jessup AT, Keller WC, Melville WK. 1990. Measurements of sea spikes in microwave backscatter at moderate incidence. *J. Geophys. Res.* 95:9679–88

Jessup AT, Melville WK, Keller WC. 1991a. Breaking waves affecting microwave backscatter. 1. Detection and verification. *J. Geophys. Res.* 96:20,547–59

Jessup AT, Melville WK, Keller WC. 1991b. Breaking waves affecting microwave backscatter. 2. Dependence on wind and wave conditions. *J. Geophys. Res.* 96:20,561–69

Kawai S, Okada K, Toba Y. 1977. Field data support of three-seconds power law and $gu_*\sigma^{-4}$-spectral form for growing wind waves. *J. Oceanogr. Soc. Jpn.* 33:137–50

Keeling RF. 1993. On the role of large bubbles in air-sea gas exchange and supersaturation in the ocean. *J. Mar. Res.* 51:237–71

Keller WC, Plant WJ, Valenzuela GR. 1986. Observations of breaking ocean waves with coherent microwave radar. In *Wave Dynamics and Radio Probing of the Sea Surface,* ed. OM Phillips, K Hasselmann, pp. 285–93. New York: Plenum

Kennedy RM. 1992. Sea surface dipole sound source dependence on wave-breaking variables. *J. Acous. Soc. Am.* 91:1974–82

Kennedy RM. 1993. Acoustic radiation due to surface wave breaking. *J. Acous. Soc. Am.* 94:2443–45

Kerman BR, ed. 1988. *Sea Surface Sound— Natural Mechanisms of Surface Generated Noise in the Ocean.* Dordrecht: Kluwer. 639 pp.

Khoo BC, Sonin AA. 1992. Augmented gas exchange across wind-sheared and shear-free air-water interfaces. *J. Geophys. Res.* 97:14,413–16

Kitaigorodskii SA. 1983. On the theory of the equilibrium range in the spectrum of wind-generated gravity waves. *J. Phys. Oceanogr.* 13:816–27

Kitaigorodskii SA. 1984. On the fluid dynamical theory of turbulent gas transfer across an air-sea interface in the presence of breaking wind-waves. *J. Phys. Oceanogr.* 14:960–72

Kitaigorodskii SA, Donelan MA, Lumley JL, Terray EA. 1983. Wave-turbulence interactions in the upper ocean. Part II. *J. Phys. Oceanogr.* 13:1988–99

Komen GJ, Cavaleri L, Donelan M, Hasselmann K, Hasselmann S, Janssen PAEM. 1994. *Dynamics and Modelling of Ocean Waves.* Cambridge: Cambridge Univ. Press. 532 pp.

Komen GJ, Hasselmann S, Hasselmann K. 1984. On the existence of a fully developed wind-sea spectrum. *J. Phys. Oceanogr.* 14:1271–85

Lamarre E. 1993. *An experimental study of air entrainment by breaking waves.* PhD Thesis. MIT/WHOI Joint Program, Cambridge/Woods Hole, MA. 327 pp.

Lamarre E, Melville WK. 1991. Air entrainment and dissipation in breaking waves. *Nature* 351:469–72

Lamarre E, Melville WK. 1992. Instrumentation for the measurement of void fraction in breaking waves: laboratory and field results. *IEEE J. Ocean. Eng.* 17:204–15

Lamarre E, Melville WK. 1994. Void-fraction measurements and sound speed fields in bubble plumes generated by breaking waves. *J. Acous. Soc. Am.* 95:1317–28

Lamont JC, Scott DS. 1970. An eddy cell model of mass transfer into the surface of a turbulent liquid. *AIChE J.* 16:513–19

Leighton TG. 1994. *The Acoustic Bubble.* New York: Academic. 613 pp.

Lighthill MJ. 1965. Contributions to the theory of waves in nonlinear dispersive systems. *J.*

Inst. Math Appl. 1:269–306

Lin JC, Rockwell D. 1994. Instantaneous structure of a breaking wave. *Phys. Fluids* 6:2877–79

Lin JC, Rockwell D. 1995. Evolution of a quasi-steady breaking wave. *J. Fluid Mech.* In press

Liss PS. 1988. Tracers of air-sea gas exchange. *Phil. Trans. R. Soc. London Ser. A* 325:93–103

Liss PS, Merlivat L. 1986. Air-sea gas exchange: introduction and synthesis. In *The Role of Air-Sea Exchange in Geochemical Cycling,* ed. P Buat-Menard, pp. 113–27. Dordrecht: Reidel. 549 pp.

Loewen MR, Melville WK. 1991a. Microwave backscatter and acoustic radiation from breaking waves. *J. Fluid Mech.* 224:601–23

Loewen MR, Melville WK. 1991b. A model of the sound generated by breaking waves. *J. Acous Soc. Am.* 90:2075–80

Loewen MR, Melville WK. 1994. An experimental investigation of collective oscillations of bubble plumes entrained by breaking waves. *J. Acous. Soc. Am.* 95:1329–43

Longuet-Higgins MS. 1974. Breaking waves in deep or shallow water. In *Proc. 10th Conf. on Naval Hydrodynamics,* MIT, pp. 597–605. Washinton DC: US Govt. Print. Office. 792 pp.

Longuet-Higgins MS. 1987. The propagation of short surface waves on longer gravity waves. *J. Fluid Mech.* 177:293–306

Longuet-Higgins MS. 1988. Mechanisms of wave breaking in deep water. See Kerman 1988, pp. 1–30

Longuet-Higgins MS. 1992. Capillary rollers and bores. *J. Fluid Mech.* 240:659–79

Longuet-Higgins MS. 1994. Shear instability in spilling breakers. *Proc. R. Soc. London Ser. A* 446:399–409

Longuet-Higgins MS. 1995. Parasitic capillary waves: a direct calculation. *J. Fluid Mech.* Submitted

Longuet-Higgins MS, Cleaver RP. 1994. Crest instabilities of gravity waves. 1. The almost highest wave. *J. Fluid Mech.* 258:115–29

Longuet-Higgins MS, Cleaver RP, Fox MJH. 1994. Crest instabilities of gravity waves. 2. Matching and asymptotic analysis. *J. Fluid Mech.* 259:333–44

Longuet-Higgins MS, Cokelet ED. 1978. The deformation of steep surface waves on water II. Growth of normal mode instabilities. *Proc. R. Soc. London Ser. A* 364:1–28

Longuet-Higgins MS, Smith ND. 1983. Measurements of breaking waves by a surface jump meter. *J. Geophys. Res.* 88:9823–31

Longuet-Higgins MS, Stewart RW. 1960. Changes in the form of short gravity waves on long waves and tidal currents. *J. Fluid*

Mech. 8:565–83

Longuet-Higgins MS, Stewart RW. 1964. Radiation stress in water waves: a physical discussion with applications. *Deep-Sea Res.* 11:529–62

Longuet-Higgins MS, Ursell F. 1948. Seawaves and microseisms. *Nature* 162:700

McLean JW, Ma YC, Martin DU, Saffman PG, Yuen HC. 1981. Three-dimensional instability of finite-amplitude water waves. *Phys. Rev. Lett.* 46:817–20

Medwin H, Beaky MM. 1989. Bubble sources of the Knudsen Sea noise spectrum. *J. Acous. Soc. Am.* 86:1124–30

Medwin H, Daniel AC. 1990. Acoustical measurement of bubble production by spilling breakers. *J. Acous. Soc. Am.* 88:40,812

Melville WK. 1982. The instability and breaking of deep-water waves. *J. Fluid Mech.* 115:163–85

Melville WK. 1983. Wave modulation and breakdown. *J. Fluid Mech.* 128:489–506

Melville WK. 1993. The role of wave breaking in air-sea interaction. In *Theoretical and Applied Mechanics, 1992: Proc. 15th Int. Congr. Theoret. Appl. Math., Haifa, Israel,* ed SR Bodner, J Singer, A Solan, Z Hashin, pp. 99–117. Amsterdam/New York: Elsevier

Melville WK. 1994. Energy dissipation by breaking waves. *J. Phys. Oceanogr.* 24:2041–49

Melville WK, Loewen MR, Felizardo FC, Jessup AT, Buckingham MJ. 1988. Acoustic and microwave signatures of breaking waves. *Nature* 336:54–59

Melville WK, Rapp RJ. 1985. Momentum flux in breaking waves. *Nature* 317:514–16; see also cover photograph

Melville WK, Rapp RJ. 1988. The surface velocity field in steep and breaking waves. *J. Fluid Mech.* 189:1–22

Merlivat L, Memery L. 1983. Gas exchange across an air-water interface: experimental results and modeling of bubble contribution to transfer. *J. Geophys. Res.* 88:707–24

Miche A. 1944. Mouvements ondulatoires de la mer en profondeur constante ou decroissante. *Ann. Ponts Chaussees,* pp. 25–78, 131–64, 270–92, 369–406

Miles JW. 1957. On the generation of surface waves by shear flows, Part I. *J. Fluid Mech.* 3:185–204

Miles J. 1993. Surface-wave generation revisited. *J. Fluid Mech.* 256:427–41

Miller RL. 1976. Role of vortices in surf zone prediction: sedimentation and wave forces. In *Beach and Nearshore Sedimentation,* ed. RA Davis, RL Ethington, pp. 92–114. Tulsa: Soc. Econ. Paleontol. Mineral. 187 pp.

Miller SJ, Shemdin OH, Longuet-Higgins

MS. 1991. Laboratory measurements of short-wave slopes on long surface waves. *J. Fluid Mech.* 233:389–404

Minnaert M. 1933. On musical air bubbles and the sounds of running water. *Phil. Mag.* 16:235–48

Mitsuyasu H. 1985. A note on the momentum transfer from wind to waves. *J. Geophys. Res.* 90:3343–45

Monahan EC, McNiocaill G, eds. 1986. *Ocean Whitecaps and Their Role in Air-Sea Exchange Processes.* Dordrecht: Reidel. 294 pp.

Oakey NS, Elliot JA. 1982. Dissipation within the surface mixed layer. *J. Phys. Ocean.* 12:171–85

Oguz HN. 1994. A theoretical study of low-frequency oceanic ambient noise. *J. Acous. Soc. Am.* 95:1895–912

Osborne AR, Burch TL. 1980. Internal solitons in the Andaman Sea. *Science* 208:451–59; see also cover photograph

Phillips OM. 1958. The equilibrium range in the spectrum of wind-generated ocean waves. *J. Fluid Mech.* 4:426–34

Phillips OM. 1960. On the dynamics of unsteady gravity waves of finite amplitude. Part 1. *J. Fluid Mech.* 9:193–217

Phillips OM. 1977. *The Dynamics of the Upper Ocean.* Cambridge: Cambridge Univ. Press. 336 pp. 2nd ed.

Phillips OM. 1981. The dispersion of short wavelets in the presence of a dominant long wave. *J. Fluid Mech.* 107:465–85

Phillips OM. 1985. Spectral and statistical properties of the equilibrium range in wind-generated gravity waves. *J. Fluid Mech.* 156:505–31

Phillips OM. 1988. Radar returns from the sea surface—Bragg scattering and breaking waves. *J. Phys. Oceanogr.* 18:1065–74

Pierson WJ, Moskowitz L. 1964. A proposed spectral form for fully-developed wind seas based on the similarity theory of SA Kitaigorodskii. *J. Geophys. Res.* 69:5191–203

Pinkel R, Smith JA. 1987. Open ocean surface wave measurement using Doppler sonar. *J. Geophys. Res.* 92:12,967–73

Plant WJ. 1982. A relationship between wind stress and wave slope. *J. Geophys. Res.* 87:1961–67

Prosperetti A. 1988. Bubble dynamics in oceanic ambient noise. See Kerman 1988, pp. 151–71

Rapp RJ, Melville WK. 1990. Laboratory measurements of deep-water breaking waves. *Phil. Trans. R. Soc. London Ser. A* 331:735–800

Smith MJ, Poulter EM, McGregor JA. 1995. Doppler radar measurements of wave groups and breaking waves. *J. Geophys. Res.* Submitted

Snyder RL, Dobson FW, Elliott JA, Long RB. 1981. Array measurements of atmospheric pressure fluctuations above surface gravity waves. *J. Fluid Mech.* 102:1–59

Spitzer WS, Jenkins WJ. 1989. Rates of vertical mixing, gas exchange and new production: estimates from seasonal gas cycles in the upper ocean. *J. Mar. Res.* 47:169–96

Stokes GG. 1847. On the theory of oscillatory waves. *Trans. Cambridge. Phil. Soc.* 8:441–55

Su M-Y, Bergin M, Marlev P, Myrick RJ. 1982. Experiments on nonlinear instabilities and evolution of steep gravity-wave trains. *J. Fluid Mech.* 124:4572

Terray AM, Agrawal YC, Drennan WM, Kahma KK, Williams AJ III, et al. 1995. Estimates of kinetic energy dissipation under breaking waves. *J. Phys. Oceanogr.* In press

Thorpe SA. 1982. On the clouds of bubbles formed by breaking wind waves in deep water, and their role in air-sea gas transfer. *Phil. Trans. R. Soc. London Ser. A* 304:155–210

Thorpe SA. 1984. The role of bubbles produced by breaking waves in supersaturating the near-surface ocean mixing layer with oxygen. *Ann. Geophys.* 2:53–56

Thorpe SA. 1985. Small-scale processes in the upper ocean boundary layer. *Nature* 318:519–22

Thorpe SA. 1992. Bubble clouds and the dynamics of the upper ocean. *Q. J. R. Meteorol. Soc.* 118:1–22

Thorpe SA. 1993. Energy loss by breaking waves. *J. Phys. Oceanogr.* 23:2498–502

Thorpe SA. 1995. Dynamical processes of transfer at the sea surface. *Prog. Oceanogr.* 35(4): In press

Thorpe SA, Hall AJ. 1983. The characteristics of breaking waves, bubble clouds and near-surface currents observed using side-scan sonar. *Cont. Shelf Res.* 1:353–84

Thorpe SA, Humphries PN. 1980. Bubbles and breaking waves. *Nature* 283:463–65

Toba Y. 1973. Local balance in the air-sea boundary processes. III. On the spectrum of wind waves. *J. Oceanogr. Soc. Jpn.* 29:209–20

Trulsen K, Dysthe KB. 1992. Action of wind-stress and breaking on the evolution of a wavetrain. In *Breaking Waves: IUTAM Symp. Sydney, Australia 1991,* ed. ML Banner, RHJ Grimshaw, pp. 243–49. Berlin/Heidelberg: Springer-Verlag. 387 pp.

Vagle S, Farmer DM. 1992. The measurement of bubble-size distributions by acoustical backscatter. *J. Atmos. Ocean. Tech.* 9:630–44

Vagle S, Large WG, Farmer DM. 1990. An evaluation of the WOTAN technique for inferring oceanic winds from underwater ambient sound. *J. Atmos. Ocean. Tech.* 7:576–95

Wallace DWR, Wirick CD. 1992. Large air-sea fluxes associated with breaking waves. *Nature* 356:694–96

Watson AJ, Upstill-Goddard RC, Liss PS. 1991. Air-sea gas exchange in rough and stormy seas measured by a dual-tracer technique. *Nature* 349:145–47

Weissman MA, Katsaros KB, Atakturk SS. 1984. Detection of breaking events in a wind-generated wave field. *J. Phys. Oceanogr.* 14:1608–19

Wenz GM. 1962. Acoustic ambient noise in the ocean: spectra and sources. *J. Acous. Soc. Am.* 34:1936–56

Woolf DK. 1993. Bubbles and the air-sea transfer velocity of gases. *Atmos. Ocean* 31:517–40

Woolf DK, Thorpe, SA. 1991. Bubbles and the air-sea exchange of gases in near-saturation conditions. *J. Mar. Res.* 49:435–66

Wu JZ. 1995. A theory of three-dimensional interfacial vorticity dynamics. *Univ. Tenn. Space Inst. Rep. 95-01,* Tullahoma, TN

Yuen HC, Lake BM. 1980. Instabilities of waves on deep water. *Annu. Rev. Fluid Mech.* 12:303–34

Zhang J, Melville WK. 1990. Evolution of weakly nonlinear short waves riding on long gravity waves. *J. Fluid Mech.* 214:321–46

Zhang J, Melville WK. 1992. On the stability of weakly nonlinear short waves on finite-amplitude long gravity waves. *J. Fluid Mech.* 243:51–72